Journal of Geochemical Exploration 133 (2013) 68–87

Contents lists available at ScienceDirect

Journal of Geochemical Exploration

journal homepage: www.elsevier.com/locate/jgeoexp

Material source analysis and element geochemical research about two types of representative bauxite deposits and terra rossa in western Guangxi, southern China

Wei Xiao [a,c], Ji Hongbing [a,b,*], Li Daojing [a,c], Zhang Fenglei [a,c], Wang Shijie [a]

[a] State Key Laboratory of Environmental Geochemistry, Institute of Geochemistry, Chinese Academy of Sciences, Guiyang 550002, China
[b] Civil and Environmental Engineering School, University of Science and Technology Beijing, Beijing 100083, China
[c] Graduate University of the Chinese Academy of Sciences, Beijing 100049, China

ARTICLE INFO

Article history:
Received 16 August 2012
Accepted 20 July 2013
Available online 1 August 2013

Keywords:
Karst-type bauxite
Terra rossa
Material source
Geochemical characteristic
Guangxi
China

ABSTRACT

In this study, geologic field observations and geochemical indicators of the types of representative bauxite deposits, terra rossa and underlying carbonate rocks in western Guangxi, southern China, were investigated. Their interrelations, material sources, formation and evolution processes were discussed. The results show an inherited relationship between terra rossa and its underlying limestone. The relevant parameter diagrams of trace and rare earth elements suggest that the two types of bauxite deposits probably possess identical material sources. Both bauxite deposits and terra rossa have close affinities with each other, implying that carbonate rocks similar to the underlying limestone might be a major material source for their formation. However, the eolian component represented by Chinese loess and igneous rock genesis with respect to Emeishan basalt plume may not contribute so much to the material source of bauxite deposits and terra rossa. In the process of leaching and pedogenesis, the mobile elements, such as Ca, Mg and Na, were preferentially dissolved and removed from parent rocks, and the less mobile elements Al, Fe, Ti and Si were accumulated and enriched. During the period of diagenesis and bauxitization, elements K and Si were largely removed from the system. Especially, in transformation from primary bauxite to secondary bauxite deposit, the contents of many "less mobile" elements, such as Fe and Ti, decreased. This finding is possibly due to the strongly acidic environment caused by decomposition of pyrite in primary sedimentation-type bauxite deposit. This study systematically analyzed the inherited relations and evolution processes among carbonate rock, terra rossa, and two types of bauxite deposits, and gave a guide for the bauxite deposit prospecting in western Guangxi.

1. Introduction

Bauxite deposits have numerous material sources (Brimhall et al., 1988; Calagari and Abedini, 2007; Chen and Lan, 1991; Deng et al., 2010; Galović et al., 2012; Liu et al., 2010; Lyew-Ayee, 1986; MacLean et al., 1997; Morelli et al., 2000; Wu and Yao, 1997). However, because the formation of bauxite deposit experiences prolonged weathering, laterization and bauxitization, most primary minerals are decomposed and destroyed, and many secondary minerals are formed. Most elements have been fractionated. For this reason, the issue of bauxite deposit material source has become a critical problem in bauxite deposit studies. In western Guangxi, one view suggests that the underlying carbonate rocks provide materials for the formation of bauxite deposits. Unfortunately, it lacks visual field observation evidence and systematical geochemistry data, so there are also some other standpoints which support that the material sources of bauxite deposits in western Guangxi are associated with archicontinent pelite or eolian origin (e.g. Chinese loess) (Wang et al., 2004; Yu et al., 2011). Deng et al. (Deng et al., 2010; Liu et al., 2010) have proposed that igneous rocks related with Emeishan basalt may be another main source of bauxite deposits.

In the past, the term "terra rossa" was a common indicator for all limestone-derived red soils in the Mediterranean region. Today, terra rossa is generally defined as a kind of reddish clayey to silty-clayey material, which occurs above limestone and dolomite in the form of a discontinuous layer, ranging from a few centimeters to several meters in thickness. It is also found in cracks and between bedding surfaces of limestone and dolomite (Durn, 2003; Feng et al., 2011). The properties and relationships between terra rossa and the underling carbonate rocks are long-standing controversial issues (Sušteršič et al., 2009). Thus it gave rise to different opinions with respect to the parent material and origin of terra rossa (Muhs and Budahn, 2009). There have been two distinguished theories of terra rossa formation, namely "residual" and "detrital" theories. The "residual" theory proposed that in-situ weathering of the local bed rock provides a major portion of source material for terra rossa (Ji et al., 2004a, b; Li and Zhu, 2004; Liu et al., 2004a; Moresi and Mongelli, 1988). According to the "detrital" theory, terra rossa formed by accumulation of allogenic materials, such as alluvial

* Corresponding author at: State Key Laboratory of Environmental Geochemistry, Institute of Geochemistry, Chinese Academy of Sciences, Guiyang 550002, China.
E-mail address: hongbing_ji@163.com (H. Ji).

0375-6742/$ – see front matter © 2013 Elsevier B.V. All rights reserved.
http://dx.doi.org/10.1016/j.gexplo.2013.07.010

mud, volcanic ash, and eolian dust (Muhs and Budahn, 2009). However, both of them have problems and limitations (Lucke, 2007; Lucke et al., 2012; Merino and Banerjee, 2008). More recently, on the basis of studies of the reaction front of bedrock and terra rossa, another theory of terra rossa formation was popular. This theory based on field and petrographic evidence stated that isovolumetric replacement seems a more universal process generated at a narrow reaction front, and dissolution of eolian dust provides major elements, such as Al, Fe and Si, to the isovolumetric reactions (Banerjee and Merino, 2011; Li et al., 1991, 1995, 2002; Merino and Banerjee, 2008).

Rock weathering, soil formation and sediment deposition are the most significant supergene geological processes in which various elements experience cycling in these geological bodies and achieve redistribution, and the geological bodies have also inherited certain particular geochemical characteristics (Ji et al., 2004a). These characteristics have been used to study the inherited relationships between weathering products and parent rocks. Most research works mainly focus upon the material sources of weathering soil or sedimentation ore deposits. However, we need to pay more attention to the study of their inherited relationships. In the investigations of the material sources and formation processes of terra rossa and bauxite deposits, the major and trace element geochemical methods have become the indispensable approaches (Esmaily et al., 2009; Ji et al., 2004a,b; Karadağ et al., 2009; MacLean et al., 1997; Meshram and Randive, 2011; Mordberg, 1993; Muhs and Budahn, 2006; Temur et al., 2009). Much attention has been paid to the similarities in major and trace elements for the potential material sources and weathering products, but little concern is given to the geochemical properties of these elements as well as the factors leading to these similarities (Liu and Qin, 1991).

Terra rossa and bauxite deposits in western Guangxi are widely distributed on Permian carbonate rocks. In this paper, the weathering soil-terra rossa, sedimentation deposit–bauxite deposit and underlying carbonate rock are discussed together. On the basis of systematical study about distribution regularities of major, trace and rare earth elements and mineral occurrence states in the geological bodies, the inherited relationship and identical material source of bauxite deposits and terra rossa are attempted to be explored. Besides, the concentration and distribution characteristics of special elements are analyzed in order to reveal the formation processes and evolutionary history of bauxite deposits.

2. Regional and deposit geology setting

The study region, which is the main bauxite producer of China, is located in western Guangxi province (Fig. 1A). The Cambrian, Devonian, Carboniferous, Permian, Triassic, Cretaceous, and Quaternary strata are mainly exposed on the Earth surface. The Devonian sandstone, shale and carbonate rocks are extensively distributed in this region, followed by Carboniferous and Permian carbonate rocks. Other strata and rocks are of limited exposure (Fig. 1C). However, the strata related with Emeishan basalt extend from Sichuan Province toward both Guizhou and Yunnan provinces, and a few of them are distributed in the northern and western parts of the study region (Fig. 1B).

The marine environment dominated this region since the Cambrian. Extensive uplift took place from the Caledonian period to Devonian. In the Early Devonian, large-scale transgression changed this region into marine again. Until the end of the Early Permian, the western Guangxi area uplifted and was denuded widely. In the Late Permian, transgressions made here become a coastal–neritic environment accepting precipitation. In the end of Triassic, Indosinian movement made this region become a land which suffered from erosion and denudation till now.

The bauxite deposits in western Guangxi occur above the Permian carbonate rocks, thus they are designated to the karst-type bauxite deposit (Deng et al., 2010; Mameli et al., 2007). However, in terms of their occurrence forms, they are divided into the primary sedimentation and the collapse-accumulation types. The thick-layered and plate-shaped sedimentation bauxite ore bodies exist in the underlying Maokou Formation (P_2m) limestone with a thickness range of 3–10 m. The contact relationship between the sedimentation bauxite deposits and the carbonate rocks is of parallel unconformity. The sedimentation bauxite ore bodies containing a minor amount of pyrite exhibit pisolitic and olitic structures, and are dense and hard. Generally, thin-layered clastic rocks are interbedded between the deposit roof (and baseplate) and carbonate rock contact zone, and the deposit roof is covered by the Heshan Formation (P_2h) carbonate rocks (Fig. 2). The accumulation type bauxite deposits and terra rossa are accumulated together in the karst depression and valley. The underlying Maokou Formation limestone underwent a long period of erosion, thus occurring as fangs in form. The bauxite ores are usually angular and clastic in shape and are not uniform in size (mostly concentrated among 1 to 10 cm). The bauxite ores are mostly reddish-brown, dark red and grayish-white in color owing to different weathering degrees. The ferricrete is discovered in the terra rossa profile (Fig. 3).

3. Sampling and analytical methods

3.1. Profile and sampling

The DJ profile (samples DJ-1 to DJ-11, location: N23°17′28.7″, E106°16′12.4″, Figs. 1C and 2) at Dajia Village, Jingxi County, Guangxi province was selected as the representative profile for the study of sedimentation-type bauxite deposits. The BY profile (samples BY-0 to BY-3, location: N23°17′4.0″, E106°16′55.7″, Figs. 1C and 4A) at the Baiyan Village, Xinjia Town, Jingxi County and the FS profile (samples FS-1 to FS-3, location: N22°14′52.7″, E107°35′13.3″) in Fusui County of Zhongzuo City were selected for comparative studies.

The ND and PG3 profiles (ND profile, samples ND-1 to ND-9, location: N23°20′49.3″, E107°32′17.7″, Figs. 1C and 4B; PG3 profile, samples PG3LT-1 to PG3LT-3, location: N23°27′31.6″, E107°26′4.2″, Fig. 1C) in northwest Pingguo County were chosen for the study of accumulation bauxite deposits. The XKC1–XKC3 dressed-by-washing accumulation bauxite ore at the dressing mill of the Pingguo Aluminum Plant was also collected for comparative studies. The PG2 profile (samples PG2-1 to PG2-11, location: N23°24′20.5″, E107°29′57.1″, Figs. 1C and 3) near the Pingguo bauxite deposit at Xingmian Village was chosen as a typical profile for the study of terra rossa. When collecting the accumulation-type bauxite ore samples, gravel-shaped bauxite deposits differing in diameter were selected randomly in the terra rossa profile. When the soil was collected, the surface soil which was affected by subsides (including dry and wet subsides) and weathering was removed. The channeling sampling method was adopted to collect samples from bottom to top. The visual profile and samples were described in sketches (Figs. 2, 3 and 4).

3.2. Experimental and chemical analysis methods

The rock and soil samples which were used for the whole-rock geochemical analysis were ground into the particle size of 200 meshes by means of a ball mill and an agate mortar. The test element (including major, trace and rare earth elements) data of all samples were provided by Beijing Research Institute of Uranium Geology. The contents of major elements in the whole-rock samples (including 12 indicators) were measured by X-ray fluorescence spectrography (XRF) by using the Philips PW2404 X-ray fluorescence spectrometer and referring the GB/T14506.28–93 silicate rock chemical analytical procedure. The trace and rare earth element concentrations were measured by Inductively Coupled Plasma Mass Spectroscopy (HR-ICP-MS) (Element I, Finnigan MAT Company) according to DZ/T0223-2001 ICP-MS procedure at a temperature of 20 °C and humidity of 30%.

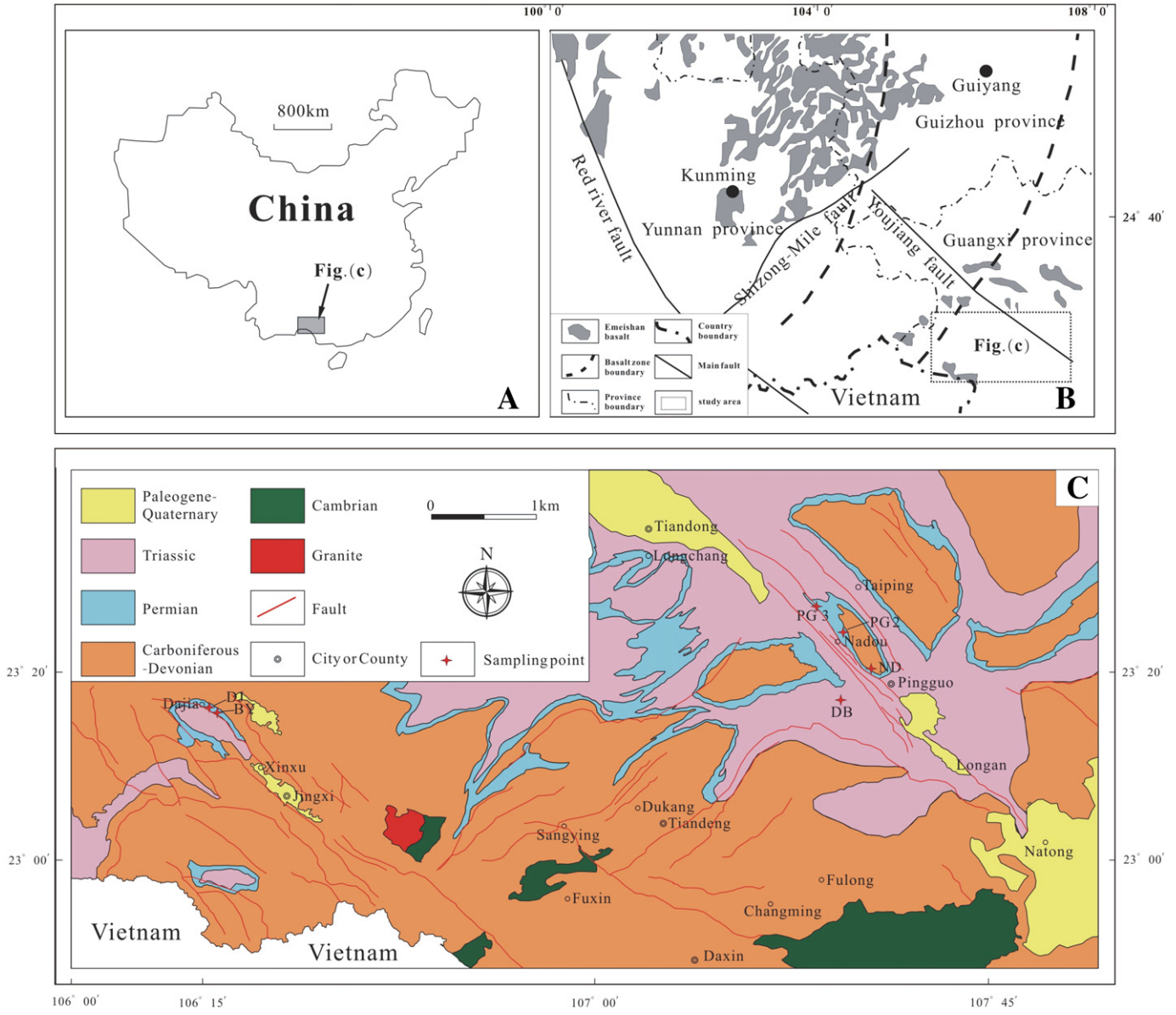

Fig. 1. (A) Administrative district map showing the location of western Guangxi, China. (B) Plot of the Emeishan basalt distribution (after Deng et al., 2010). (C) Geologic sketch of western Guangxi.

4. Results

4.1. Major element geochemical characteristics

The major element concentrations of samples from study profiles in western Guangxi are listed in Table 1. As viewed from Table 1, the oxides Al_2O_3, SiO_2, Fe_2O_3 and LOI, which account for 95% of the total rock mass, and the others are quite low. Bauxite deposits are characterized by enrichment of Al_2O_3 and depletion of SiO_2 and Fe_2O_3, whereas, in terra rossa, the three kinds of oxides have similar concentrations. The Al_2O_3 contents and A/S ratios (refer to concentration ratio of Al_2O_3 and SiO_2) of samples in accumulation bauxite, sedimentation bauxite and terra rossa decrease in sequence. Their Al_2O_3 average contents and A/S mean value are: accumulation bauxite ore, 67.26 wt.% and 16.67;sedimentation bauxite ore, 41.42 wt.% and 3.63;terra rossa, 31.25 wt.% and 1.18.

The relationship between CIA and oxides is shown in Fig. 5. The variation of oxide contents with increasing chemical alteration index indicates that: (I) The two types of bauxite deposits in the study area have higher CIA values (>99), while CIA values in the samples of terra rossa are relatively low (92–96). (II) Bauxite samples compared with terra rossa are more enriched in the stable oxides Al_2O_3, TiO_2 and Fe_2O_3, and depleted in K_2O, CaO, SiO_2 and other soluble oxides. (III) The contents of the stable oxides Al_2O_3, TiO_2 and Fe_2O_3 in terra rossa have no significant variation with the increasing of CIA (distributed as a horizontal line). However, that in bauxite deposits has obvious changes within a small interval of CIA. (IV) The concentrations of TiO_2 and Fe_2O_3 in all samples, except Al_2O_3 in sedimentation-type bauxite samples ($R^2 = 0.63$), have no visible correlation with the CIA values. As for terra rossa samples, the contents of CaO and K_2O have a negative correlation with CIA ($R^2 = 0.90$, $R^2 = 0.42$, respectively). In the sedimentation type bauxite samples, the concentrations of SiO_2, CaO and K_2O have a negative correlation with CIA ($R^2 = 0.85$, 0.93, 0.64, respectively).

The ternary diagram of $Fe_2O_3^T$–SiO_2–Al_2O_3 is generally used to explain the degree of laterization and to classify bauxite deposits. In Fig. 6A (Bardossy, 1982), the accumulation bauxite samples in the study area are located in the bauxite region, the sedimentation bauxite samples fall within the iron-rich bauxite region, the terra rossa samples

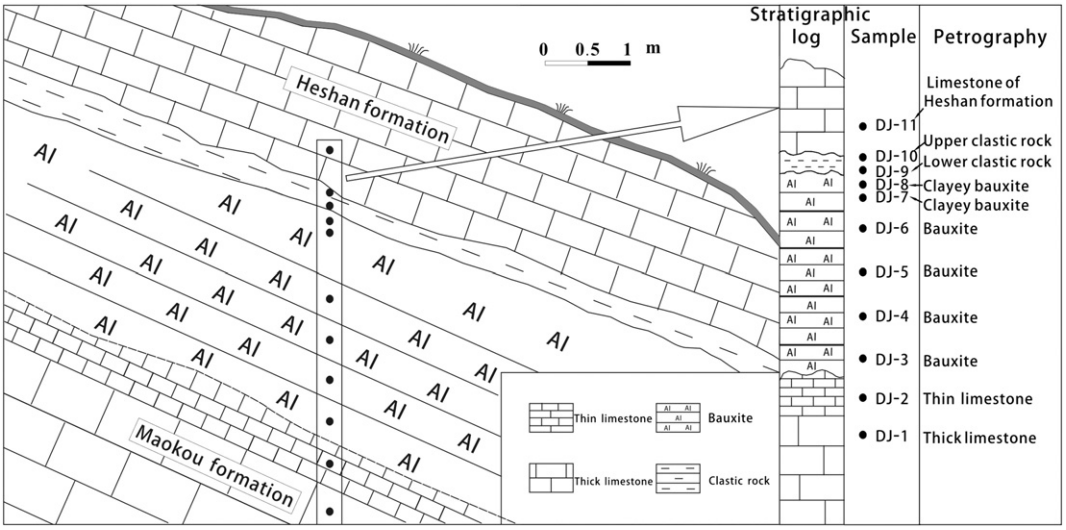

Fig. 2. Sketch and stratigraphic log of sedimentation-type bauxite deposit from the DJ profile in western Guangxi.

are from the region defined by the clayey bauxite, and the Emeishan basalt and Chinese loess samples are located in the bauxitic clay area. Schellman (1986) used the ternary diagram of $Fe_2O_3^T$–SiO_2–Al_2O_3 (Fig. 6B) to define four different laterization processes. From terra rossa to the sedimentation-type bauxite deposits to the accumulation-type bauxite deposits, the curve shows a variation process of laterization from weak to strong.

4.2. Trace element geochemical characteristics

The trace element contents are listed in Table 2. From the UCC normalized trace element spider-diagrams (Fig. 7), the characteristics are shown as follows: (I) The UCC normalized trace element distribution patterns of bauxite deposits and terra rossa are quite similar as a whole. The accumulation bauxite samples are depleted in Ni and Zn compared with the sedimentation bauxite ores. Terra rossa is slightly depleted in Nb relative to the bauxite deposits. (II) The same trace elements, especially stable elements, in samples of bauxite deposits and terra rossa have experienced no significant fractionation, while the fractionation of the same trace elements in carbonate rock samples is visible. (III) The trace element distribution patterns of the carbonate rocks are generally similar to those of bauxite deposits, especially samples DJ-1 and BY-2. However, the contents of trace elements in carbonate rocks are lower than those in bauxite deposits, and carbonate rocks are characterized by relative enrichment of Sr. The trace element distribution patterns of Emeishan basalt and Chinese loess samples are significantly different from those of bauxite ores and terra rossa. (IV) The depletion valley of the two types of bauxite deposits appears at the elements Rb, Sr, K, Ba, Na and Cd, and other stable elements, related to the UCC, are concentrated.

4.3. REE geochemical characteristics

The REE data and relevant parameters are listed in Table 3. The total REE content ($\sum$REE) has a considerable variation that range from 200 ppm to 1000 ppm, and their mean value is about 500 ppm. Samples in sedimentation bauxite deposit have significant Ce positive anomalies that vary from 1.41 to 4.47, with an average value of 3.00. However, samples of accumulation bauxite deposit and terra rossa do not have distinct Ce anomalies. In addition, all the test samples have Eu negative anomalies that range from 0.5 to 0.6.

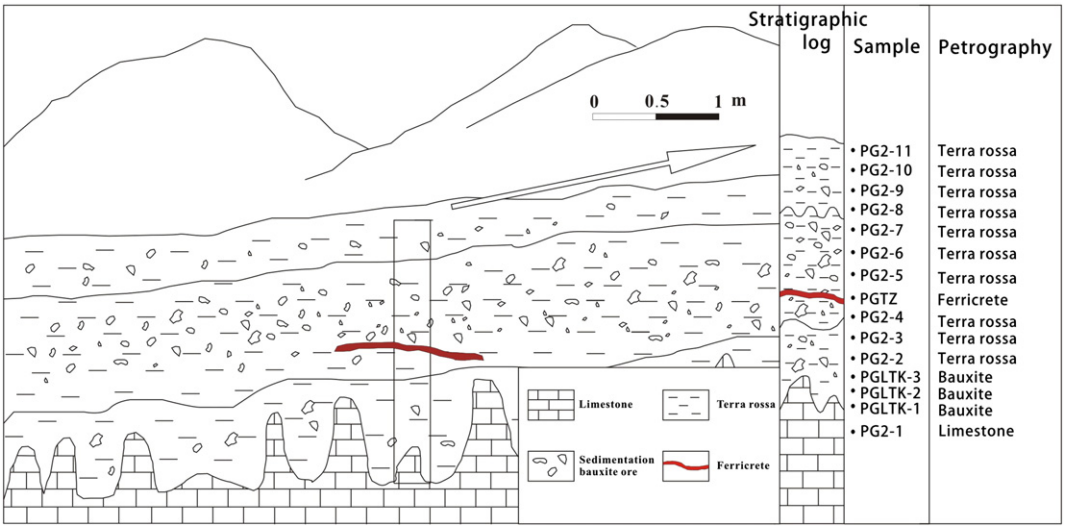

Fig. 3. Sketch and stratigraphic log of accumulation-type bauxite deposit from the PG2 profile in western Guangxi.

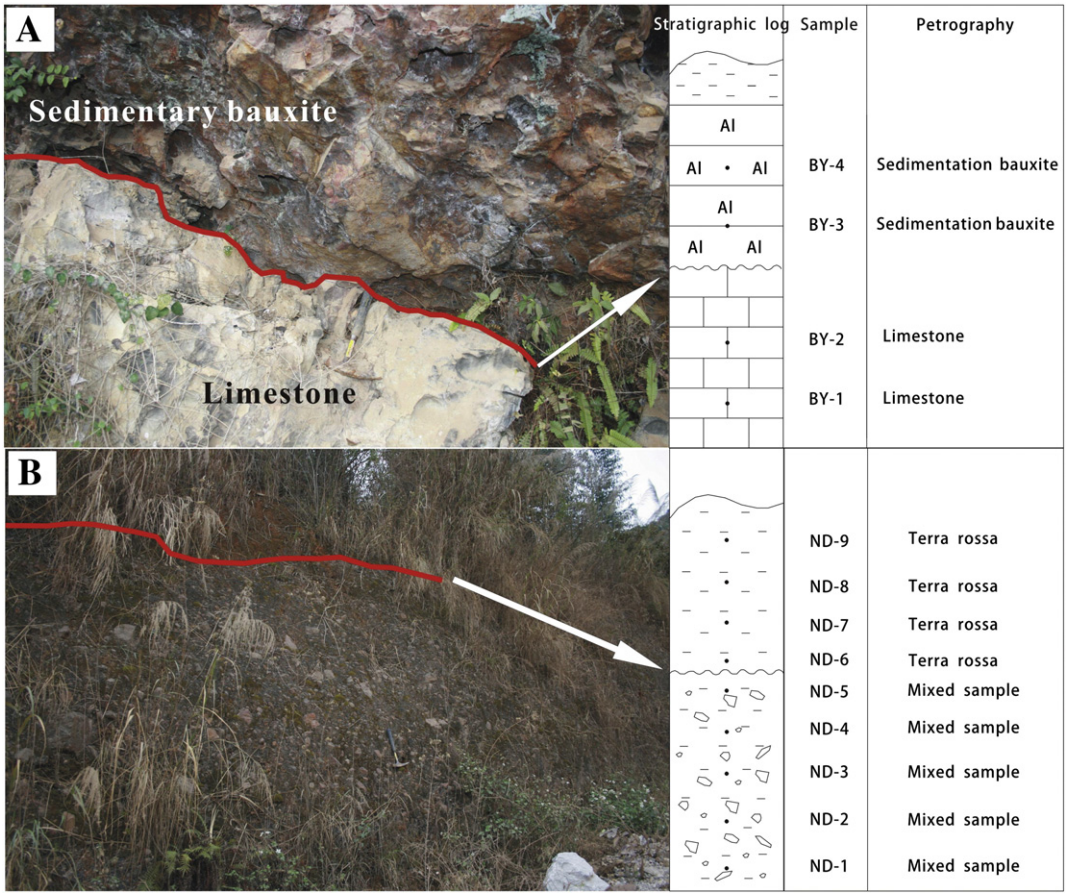

Fig. 4. (A) Photo and stratigraphic log of sedimentation-type bauxite deposits from the BY profile and (B) accumulation-type bauxites from the ND profile. The red line in (A) represents the parallel unconformity interface between sedimentation-type bauxite and the underlying limestone. The red line in (B) stands for the boundary of the overlying terra rossa and accumulation-type bauxite.

The characteristics of chondrite normalized REE patterns of samples from this region are described as follows (Fig. 8): (I) steep LREE distributions, which are generally ascribed to an enrichment of large ion lithophile element caused by the partial mantling of mantle or crustal rocks (McLennan, 1989), (II) mostly flat HREE distributions, except for Emeishan basalt samples, implying that there are no significant HREE fractionations, and (III) relatively high $\sum$REE values of bauxite deposits and terra rossa, and low values in samples of the carbonate rock, basalt and Chinese loess, which might well be associated with the dilution effect of CaO and SiO_2.

5. Discussions

5.1. Source of the two types of typical bauxite deposits and terra rossa

Many hypotheses about the material sources of bauxite deposits and terra rossa have been proposed as follows (Deng et al., 2010; Liu et al., 2010; Wang et al., 2004; Yu et al., 2011): (I) underlying Maokou carbonate rocks, (II) cratogenic pelite, (III) eolian material (e.g. Chinese loess), and (IV) igneous rocks associated with the Emeishan basalt. All of them are possible potential genesis of bauxite deposits in the study region.

5.1.1. Field observation of geology as provenance indicator

The primary sedimentation bauxite deposit presents parallel unconformity contacting with the underlying carbonate rocks, and the contact surface presents indented shape or dissolved caves rather than smooth plane (Fig. 9A and B). It is the similar situation for the contact surface of terra rossa and Permian carbonate rock. The field observation indicates that the underlying carbonate rocks had suffered from the denudation before they accepted the sedimentation of primary bauxite deposit and accumulation of terra rossa. Thereby, it is possible that the underlying carbonate rock provided a material source for them.

Accumulation bauxite ores in the thick terra rossa profiles commonly show brecciaous shapes (Fig. 9C) which indicates that they did not undergo long-distance transportation. Regional epibiotic primary sedimentation bauxite bodies are discovered to surround the karst depressions and valleys where accumulation bauxite deposit is located. In addition, both of the two types of bauxite deposits were usually found in places where Permian stratum was exposed (Fig. 1C). It indicates that accumulation bauxite deposit was possibly derived from primary sedimentation bauxite deposit. However, differences between the two types of bauxite deposits, such as construction, shapes, position and geochemical index, illustrate that the transformation process experienced intensive weathering or/and tectonic stress.

In geotectonics, the large-scale fold is created by intensive tectonic stress. Moreover, the anticline is of well developed joints attributed to the tension, and it is easily destroyed by weathering and denudation. On the contrary, the syncline is quite compact because of the extrusion force, and the ancient strata could be reserved. In western Guangxi, accumulation bauxite profiles (such as profiles PG2 and ND) were mostly located along an anticline, whereas sedimentation bauxite profiles (such as profiles DJ and BY) were commonly found in a syncline (Fig. 1C). This finding indicates that tectonic stress probably plays an important part in the formation of accumulation bauxite deposit.

5.1.2. Element distribution pattern evidences

The weathering products generally inherited certain particular geochemical characteristics of their parent materials, so the distribution

Table 1
Major element contents and CIA value of bulk samples from bauxite deposits, terra rossa and carbonate rock profiles in western Guangxi.

Samples	BY-0	BY-1	DJ-1	DJ-2	PG2-1	PG2-2	PG2-3	PG2-4	PG2-5	PG2-6	PG2-7	PG2-8	PG2-9	PG2-10	PG2-11	ND-1	ND-2	ND-3	ND-4	ND-5
Petrography	L[a]	L	L	L	L	T[a]	T	T	T	T	T	T	T	T	T	C[a]	C	C	C	C
SiO_2	0.05	0.91	1.27	0.29	0.70	24.04	24.21	24.21	24.20	24.30	24.85	24.90	25.17	25.93	24.99	25.68	27.18	23.40	25.42	24.35
Al_2O_3	0.11	1.32	1.52	0.27	0.54	31.80	31.89	31.89	32.51	32.37	31.90	31.53	31.20	31.19	31.30	35.51	32.64	34.47	32.38	32.03
$Fe_2O_3^T$	0.09	1.07	0.90	0.96	0.16	19.40	20.71	20.80	20.30	20.36	20.30	20.32	19.91	19.80	20.32	21.05	23.08	24.96	25.14	27.15
MgO	0.05	0.17	0.10	0.11	2.37	0.50	0.54	0.55	0.53	0.51	0.53	0.54	0.55	0.57	0.55	0.20	0.22	0.28	0.24	0.25
CaO	57.94	54.41	53.66	55.15	52.61	1.74	0.48	0.44	0.37	0.36	0.37	0.42	0.57	0.49	0.43	0.31	0.25	0.25	0.25	0.21
Na_2O	0.03	0.06	0.10	0.03	0.06	0.13	0.13	0.13	0.13	0.12	0.13	0.13	0.13	0.13	0.12	0.11	0.10	0.10	0.08	0.09
K_2O	0.01	0.04	0.03	0.01	0.02	0.96	0.92	0.93	0.92	0.91	0.93	0.94	1.00	1.05	0.93	0.11	0.13	0.18	0.17	0.16
MnO	–	0.03	0.01	0.02	–	0.21	0.20	0.20	0.20	0.20	0.20	0.19	0.17	0.16	0.17	0.06	0.04	0.05	0.08	0.04
TiO_2	0.01	0.11	0.13	0.01	0.03	2.42	2.41	2.37	2.42	2.39	2.28	2.24	2.14	2.07	2.16	2.85	2.55	2.61	2.49	2.55
P_2O_5	0.01	0.16	0.02	0.01	0.01	0.13	0.14	0.15	0.15	0.15	0.15	0.16	0.14	0.14	0.16	0.13	0.13	0.16	0.15	0.16
LOI	41.23	41.37	41.76	42.57	43.42	18.26	17.96	17.92	17.86	17.95	17.98	18.22	18.44	18.16	18.28	13.59	13.35	13.20	13.37	12.87
CIA[b]	–	–	–	–	–	91.8	95.1	95.5	95.8	95.8	95.7	95.5	94.8	94.9	95.4	98.5	98.6	98.5	98.5	98.6

[a] L, T, C, S and A stand for limestone, terra rossa, composite sample, sedimentary bauxite ore and accumulation bauxite ore, respectively. All the major element values are in weight percent.
[b] Chemical index of alteration (CIA) = Al_2O_3 / (Al_2O_3 + CaO^* + Na_2O + K_2O), where CaO^* only represents the Ca in silicate (Nesbitt and Young, 1982).
[c] – Means the content is under the test limit.

ND-6	ND-7	ND-8	ND-9	PG3LT-1	PG3LT-2	PG3LT-3	XKC-1	XKC-2	XKC-3	BY-2	BY-3	DJ-3	DJ-4	DJ-5	DJ-6	FS-1	FS-2	FS-3
T	T	T	T	A[a]	A	A	A	A	A	S[a]	S	S	S	S	S	S	S	S
31.33	31.81	31.75	31.45	2.63	4.36	2.65	7.21	7.01	10.38	14.58	6.73	9.47	8.18	10.09	14.70	24.33	21.38	19.48
30.09	29.92	30.05	29.97	78.27	76.04	77.86	60.89	55.57	55.57	37.64	43.70	39.73	45.85	50.61	46.09	33.45	36.80	37.68
17.54	17.32	17.51	17.55	0.29	0.72	1.16	12.09	18.49	15.23	30.12	32.94	34.63	28.46	22.90	20.59	25.44	24.30	25.37
0.48	0.50	0.51	0.49	0.10	0.11	0.10	0.17	0.15	0.14	1.34	0.38	0.17	0.18	0.27	2.83	0.21	0.18	0.19
0.28	0.30	0.29	0.27	0.11	0.11	0.12	0.38	0.24	0.09	0.15	0.14	0.08	0.11	0.10	0.08	0.42	0.24	0.22
0.11	0.11	0.11	0.10	0.18	0.36	0.09	0.13	0.08	0.14	0.07	0.07	0.04	0.06	0.06	0.10	0.10	0.13	0.15
0.63	0.66	0.63	0.61	0.03	0.04	0.03	0.08	0.09	0.13	0.03	0.03	0.01	0.02	0.02	0.05	0.06	0.08	0.08
0.07	0.07	0.07	0.07	–[c]	–	–	0.03	0.04	0.01	0.03	0.03	0.01	0.01	0.01	0.03	0.09	0.08	0.09
2.21	2.13	2.09	1.98	2.27	2.68	2.46	3.86	3.43	3.77	3.87	4.16	4.66	4.34	3.94	3.30	4.51	4.52	4.36
0.25	0.25	0.25	0.25	0.05	0.06	0.07	0.10	0.11	0.07	0.03	0.04	0.02	0.03	0.03	0.03	0.05	0.06	0.06
16.65	16.56	16.39	16.74	15.47	14.96	14.87	14.49	14.24	13.89	11.58	11.26	10.66	12.26	11.38	11.66	11.04	11.90	11.96
96.7	96.5	96.7	96.8	99.5	99.3	99.7	99.0	99.3	99.4	99.3	99.4	99.7	99.6	99.6	99.5	98.3	98.8	98.8

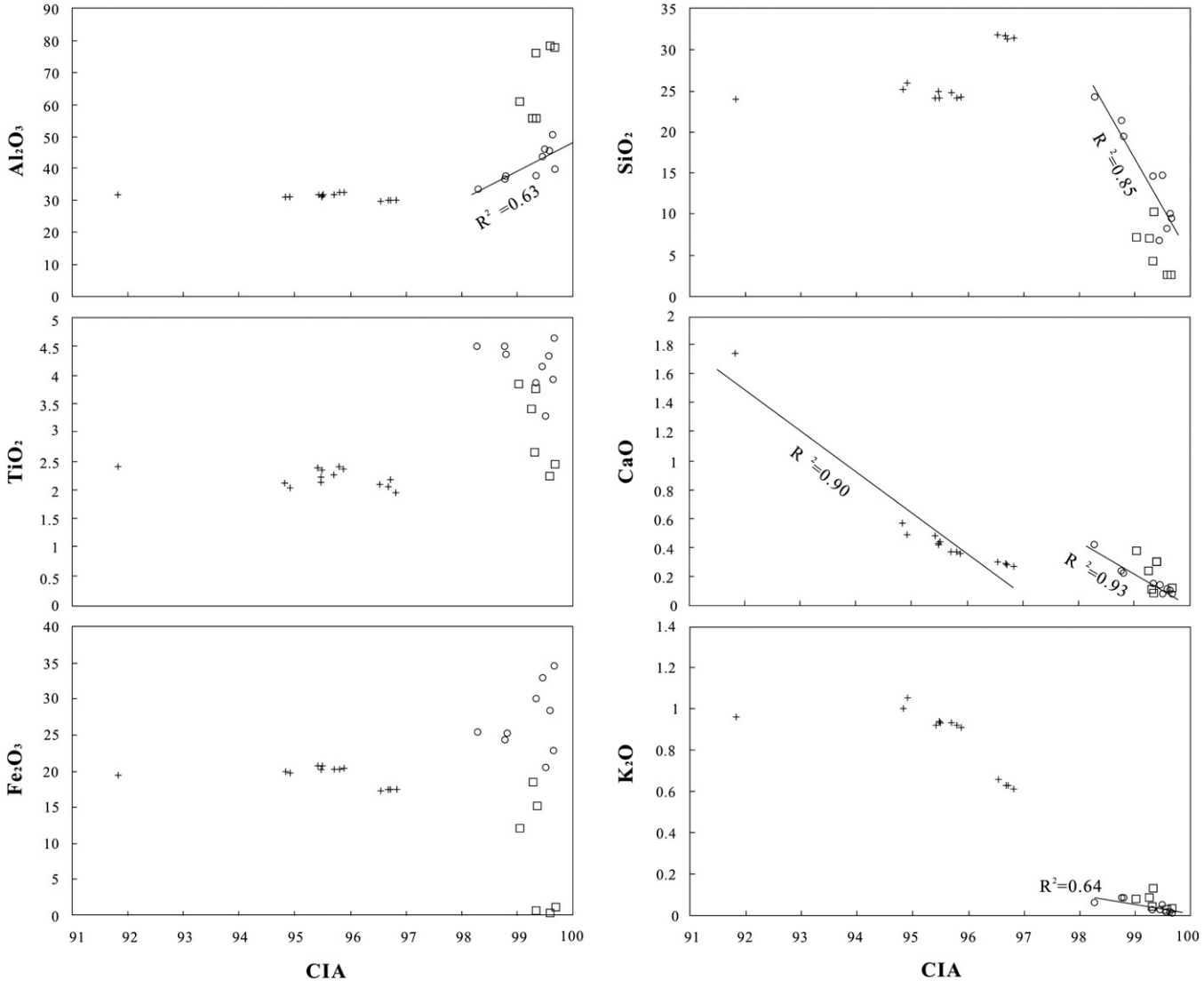

Fig. 5. Variation plots of major oxides versus CIA for the samples of sedimentation-type bauxite, accumulation-type bauxite and terra rossa. Open circles represent sedimentation-type bauxite samples, black boxes stand for accumulation-type bauxite samples, and crisscrosses represent terra rossa.

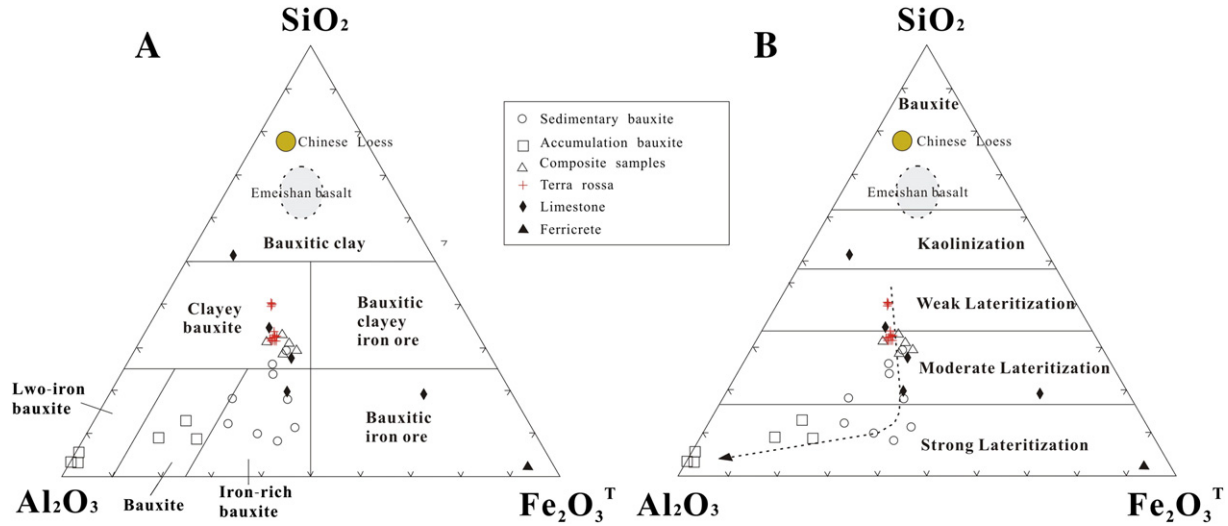

Fig. 6. Ternary diagrams of the concentrations of $Fe_2O_3^T$, SiO_2 andAl_2O_3 for study samples of western Guangxi and potential genesis. Plot (A) shows the classification of bauxites (after Bardossy, 1982), and plot (B) displays the degree of laterization (after Schellman, 1986).

Table 2
Trace element contents of bulk samples from bauxite deposits, terra rossa and carbonate rock profiles in western Guangxi.

Samples	BY-0	BY-1	DJ-1	DJ-2	PG2-1	PG2-2	PG2-3	PG2-4	PG2-5	PG2-6	PG2-7	PG2-8	PG2-9	PG2-10	PG2-11	ND-1	ND-2	ND-3	ND-4	ND-5
Petrography	L[a]	L	L	L	L	T[a]	T	T	T	T	T	T	T	T	T	C[a]	C	C	C	C
Sc	0.40	4.47	6.91	7.29	0.22	41.30	42.90	50.80	29.00	50.40	44.30	45.50	30.80	26.60	41.70	37.70	34.80	41.90	25.90	48.40
V	11.10	16.00	18.60	13.00	20.90	384.00	394.00	471.00	433.00	451.00	421.00	418.00	406.00	440.00	382.00	295.00	257.00	262.00	258.00	278.00
Cr	24.10	32.10	27.30	17.40	33.20	543.00	522.00	620.00	523.00	586.00	496.00	523.00	416.00	472.00	449.00	839.00	487.00	526.00	588.00	668.00
Co	5.56	7.01	4.60	5.10	7.65	65.20	67.90	78.50	73.00	71.40	65.40	59.10	49.10	45.60	54.90	48.90	23.20	30.00	39.30	31.00
Ni	16.00	18.40	16.00	12.50	10.20	129.00	123.00	156.00	138.00	149.00	134.00	126.00	119.00	114.00	111.00	74.40	51.40	54.40	54.10	63.80
Cu	2.28	11.00	4.02	2.15	1.53	81.50	83.20	106.00	92.30	103.00	94.90	90.80	85.00	87.50	81.00	39.20	38.20	37.20	37.90	40.70
Zn	2.75	11.50	13.80	3.14	3.26	396.00	387.00	491.00	314.00	449.00	412.00	422.00	340.00	313.00	392.00	136.00	128.00	153.00	175.00	178.00
Ga	0.09	3.81	2.76	2.25	–[b]	48.20	46.30	59.00	52.10	57.40	51.90	51.30	46.30	46.80	45.20	53.10	48.50	54.60	51.20	52.70
Rb	0.19	1.05	0.25	0.09	–	81.20	77.20	91.40	66.00	86.30	79.30	88.80	76.20	27.00	85.20	4.84	7.83	10.60	11.90	10.10
Sr	104.00	143.00	109.00	109.00	95.80	166.00	127.00	151.00	66.20	153.00	118.00	143.00	79.50	44.10	125.00	32.30	35.30	38.20	37.00	39.90
Y	3.96	69.40	36.30	43.90	0.46	128.00	140.00	163.00	69.80	108.00	85.90	119.00	74.20	43.20	97.50	108.00	91.70	110.00	110.00	192.00
Nb	0.35	6.88	5.66	0.36	0.05	58.60	63.60	73.70	71.00	73.60	61.70	58.60	53.50	52.70	51.50	106.00	85.60	97.30	91.00	95.10
Mo	0.03	0.05	0.12	0.40	–	6.01	6.34	7.80	7.24	7.42	6.75	6.61	5.95	5.68	5.46	5.84	5.46	6.04	4.63	5.66
Cd	0.19	1.68	4.00	0.81	0.11	7.59	7.40	9.36	5.88	7.11	5.70	5.96	6.68	5.33	3.98	3.43	3.38	3.48	3.62	3.56
Cs	0.05	0.05	0.04	0.01	0.02	18.70	17.70	21.00	17.30	20.70	19.50	19.70	17.70	4.51	18.50	0.88	2.17	2.91	3.21	2.61
Ba	1.97	9.47	4.86	4.36	3.87	135.00	132.00	155.00	107.00	157.00	127.00	159.00	128.00	56.30	150.00	18.40	19.80	24.60	27.20	24.10
Ta	0.03	0.47	0.38	0.03	16.80	4.30	4.43	5.10	5.11	5.11	4.49	4.19	3.92	3.82	3.61	6.83	5.44	6.26	5.78	6.11
Pb	0.09	3.00	5.29	3.52	0.38	132.00	131.00	151.00	106.00	149.00	125.00	135.00	95.60	86.00	118.00	121.00	102.00	126.00	130.00	125.00
Th	0.12	1.95	1.99	0.18	0.09	39.20	39.60	42.80	19.00	45.10	26.50	44.40	21.90	9.21	39.40	44.90	42.80	52.50	42.80	50.20
U	0.41	0.96	1.16	0.79	0.23	13.40	13.50	16.90	9.91	16.40	12.50	15.30	7.46	8.76	12.90	6.67	9.65	11.60	11.20	11.80
Zr	3.45	63.20	68.10	5.16	0.71	690.00	701.00	817.00	746.00	806.00	720.00	698.00	582.00	622.00	602.00	1055.00	864.00	965.00	935.00	992.00
Hf	0.08	1.74	1.60	0.18	0.02	18.30	19.50	23.90	21.80	3.30	20.50	19.60	16.40	16.90	17.40	32.00	26.10	31.20	28.60	30.60

[a] L, T, M, S and A stand for limestone, terra rossa, mixed sample, sedimentary bauxite ore and accumulation bauxite ore, respectively. All the trace element values are in ppm.
[b] – Means the content is under the test limit.

ND-6	ND-7	ND-8	ND-9	PG3LT-1	PG3LT-2	PG3LT-3	XKC-1	XKC-2	XKC-3	BY-2	BY-3	DJ-3	DJ-4	DJ-5	DJ-6	FS-1	FS-2	FS-3
T	T	T	T	A[a]	A	A	A	A	A	S[a]	S	S	S	S	S	S	S	S
35.90	31.70	32.10	27.50	43.00	81.70	66.00	41.20	45.70	51.60	27.40	56.20	53.30	46.90	36.60	43.70	41.60	45.80	42.60
280.00	283.00	261.00	265.00	255.00	229.00	211.00	317.00	308.00	248.00	188.00	232.00	248.00	231.00	191.00	144.00	136.00	153.00	132.00
511.00	462.00	456.00	466.00	728.00	777.00	761.00	755.00	685.00	658.00	363.00	451.00	513.00	496.00	425.00	410.00	292.00	298.00	325.00
21.60	20.00	19.30	17.00	28.40	26.40	30.20	32.20	36.10	33.20	38.30	18.00	15.20	22.00	18.90	20.10	27.30	49.20	49.20
79.80	75.90	69.40	75.80	4.64	6.82	6.49	39.80	40.80	63.10	67.60	70.30	95.70	60.10	47.80	42.20	115.00	161.00	144.00
62.30	57.90	53.70	57.30	21.30	25.20	23.60	60.50	56.80	55.10	22.90	26.40	50.10	43.50	56.20	131.00	53.90	34.30	44.10
388.00	354.00	310.00	296.00	23.90	45.60	33.60	105.00	201.00	77.20	161.00	103.00	101.00	93.70	101.00	112.00	74.00	117.00	111.00
46.50	43.80	42.20	41.70	88.20	100.00	75.00	84.80	76.10	71.50	82.60	93.50	97.10	77.90	81.60	70.80	53.40	57.90	61.00
73.20	61.80	51.90	41.70	0.46	0.82	0.65	1.52	5.38	8.06	0.09	0.15	0.17	0.06	0.10	0.38	0.97	1.11	1.42
90.80	76.60	61.80	39.80	12.80	26.70	16.90	13.10	30.00	42.10	9.42	11.10	12.10	10.30	13.50	22.40	37.30	44.70	54.10
85.10	71.70	70.60	52.20	138.00	254.00	173.00	98.50	104.00	194.00	35.30	71.40	130.00	80.80	46.30	54.10	29.50	53.40	48.60
59.30	54.20	54.00	51.50	268.00	295.00	237.00	217.00	174.00	193.00	177.00	230.00	214.00	193.00	158.00	141.00	133.00	150.00	145.00
5.03	4.74	4.42	4.44	15.30	3.97	8.11	6.12	5.63	5.19	1.07	4.30	3.53	3.52	0.88	1.76	1.63	2.09	1.79
4.26	2.62	2.39	2.51	1.51	2.06	2.04	3.75	3.76	4.31	1.98	2.11	1.79	1.84	1.34	1.30	1.43	1.60	1.45
15.90	15.30	13.40	11.60	0.15	0.22	0.26	0.08	1.26	1.84	0.03	0.01	0.27	0.44	0.07	0.34	0.14	0.06	0.16
122.00	114.00	91.70	77.30	16.90	19.80	15.50	21.00	19.60	17.00	7.79	7.61	19.40	12.80	5.40	14.30	76.80	47.50	56.00
3.86	3.52	3.61	3.39	19.00	20.50	17.80	14.10	11.50	12.60	11.80	14.80	14.40	13.00	10.70	9.50	8.83	9.71	9.40
82.40	77.60	68.20	58.00	19.80	22.50	17.30	83.00	111.00	82.40	31.70	132.00	129.00	123.00	47.00	12.30	92.40	90.70	90.80
43.90	38.60	29.30	17.00	65.90	65.80	43.00	82.30	69.00	74.00	48.40	77.80	72.20	66.30	65.40	61.20	42.30	47.90	47.30
9.70	9.43	6.00	4.25	37.70	26.10	7.79	24.30	19.30	21.00	22.60	17.30	26.30	16.30	15.40	19.40	7.00	6.59	5.49
618.00	572.00	578.00	590.00	2541.00	3019.00	2422.00	2144.00	1638.00	1851.00	1593.00	2474.00	2136.00	1873.00	1578.00	1344.00	1307.00	1395.00	1366.00
18.00	16.90	17.20	17.50	79.20	89.80	71.20	68.50	56.70	60.20	49.50	70.70	63.60	57.20	50.50	42.80	38.40	41.60	41.20

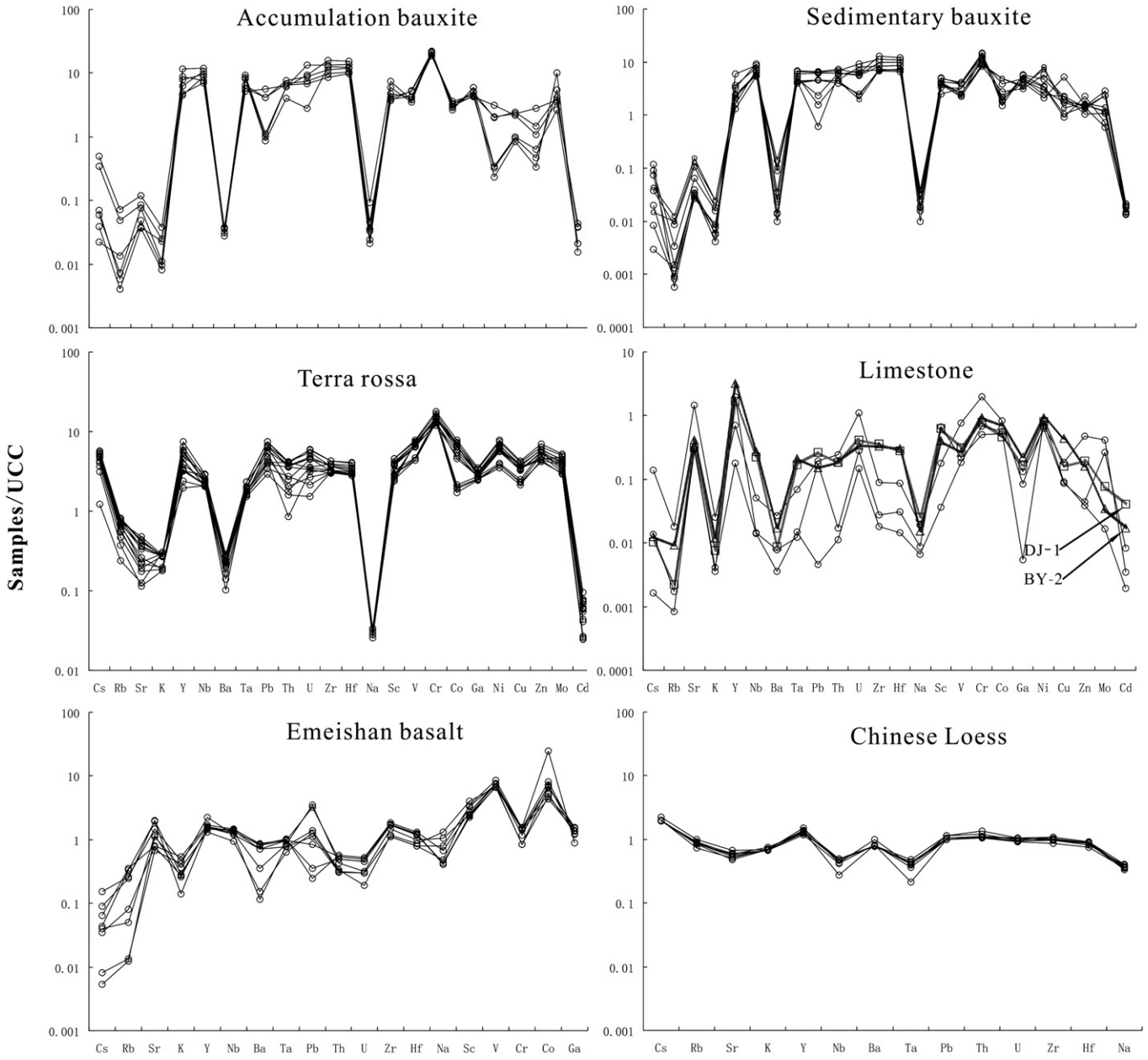

Fig. 7. UCC normalized spider-diagrams of samples of bauxite deposits, terra rossa, underlying limestone, Emeishan basalt and Chinese loess. Upper continental crust (UCC) data cited from Taylor and McLennan (1985), Chinese loess values after Ding et al. (2000) and Peucker-Ehrenbrink and Jahn (2001), and Emeishan Basalt data used here from Xu (2006) and Zhong et al. (2006).

patterns of trace elements are regarded as an excellent instrument for tracing the provenance of the weathering product (Ji et al., 2004a; Meshram and Randive, 2011).

The spider diagram of trace element distribution (Fig. 7) shows bauxite deposits and terra rossa, and individual carbonate rock samples (samples DJ-1 and BY-1) have similar overall distribution patterns of trace elements, which are different from those of Chinese loess and Emeishan basalt.

The spider diagram (Fig. 8) displays the chondrite normalized REE distribution patterns of samples of the two types of typical bauxite deposits, terra rossa and the underlying carbonate rocks, as well as Chinese loess and Emeishan basalt. The result suggests that all of these samples, except for Emeishan basalt samples, show similar REE distribution patterns characterized by steep LREE fraction, mostly flat HREE section and visible negative Eu anomaly. However, the differences of Ce anomalies are possibly caused by the redox conditions of environment rather than the inheritance of parent rocks. Since REE fractionations are related to drainage conditions (Marker and de Oliveira, 1994), while the redox conditions significantly influence the fractionations of elements Ce and Eu from others (Mongelli, 1993; Panahi et al., 2000). Whereas, the fractionation of Eu requires strong reducing conditions rarely encountered in supergene environment (Laveuf and Cornu, 2009). The differences between REE distribution patterns of Emeishan basalt and bauxite deposits are attributed to the steep HREE distributions and unobvious Eu anomalies. Besides, the HREE section of Chinese loess was slightly inclined.

The above observation indicates that there is a close affinity or inheritance among bauxite deposits, terra rossa and the underlying carbonate rocks, and that Chinese loess and Emeishan basalt have no significant inheritance with bauxite deposits in the study area.

5.1.3. Element ratio evidences

TiO_2/Al_2O_3 ratios were used to investigate the material source of sediments and sedimentation rocks (Young and Nesbitt, 1998). Similarly,

Table 3
Rare earth element contents and relative parameters of bulk samples from bauxite deposits, terra rossa and carbonate rock profiles in western Guangxi.

Samples	BY-0	BY-1	DJ-1	DJ-2	PG2-1	PG2-2	PG2-3	PG2-4	PG2-5	PG2-6	PG2-7	PG2-8	PG2-9	PG2-10	PG2-11	ND-1	ND-2	ND-3	ND-4	ND-5
Petrography	L[a]	L	L	L	L	T[a]	T	T	T	T	T	T	T	T	T	C[a]	C	C	C	C
La	0.81	35.30	29.80	23.20	0.29	121.00	116.00	135.00	95.30	110.00	94.80	109.00	99.40	45.50	103.00	118.00	76.70	92.70	91.00	128.00
Ce	1.24	29.90	32.70	35.30	0.37	254.00	244.00	295.00	205.00	284.00	232.00	258.00	184.00	156.00	235.00	545.00	360.00	614.00	487.00	267.00
Pr	0.15	6.51	7.57	5.67	0.06	29.30	28.80	34.20	21.80	24.20	21.10	25.40	23.80	10.70	22.10	15.70	13.20	15.60	16.00	21.30
Nd	0.57	23.90	31.80	21.10	0.19	116.00	122.00	140.00	87.00	92.70	84.50	97.30	96.00	41.50	84.50	54.10	49.00	56.30	59.60	80.40
Sm	0.10	5.50	6.89	5.32	0.02	25.60	27.80	32.80	19.20	22.60	19.10	24.20	19.10	8.67	19.10	10.40	10.40	11.70	13.30	18.10
Eu	0.02	0.96	1.03	0.95	0.01	4.87	5.37	6.40	3.37	4.34	3.76	4.70	3.64	1.81	3.74	1.97	1.95	2.26	2.54	3.60
Gd	0.16	6.78	7.10	5.75	0.03	23.00	24.70	27.90	14.90	19.00	16.70	20.80	16.70	8.35	17.00	13.40	11.50	14.50	14.60	19.70
Tb	0.02	1.56	1.25	1.33	0.01	4.19	4.69	5.47	2.91	4.08	3.35	4.00	2.71	1.48	3.13	2.72	2.21	2.78	2.98	4.33
Dy	0.17	9.68	6.64	7.63	0.04	24.60	26.60	31.50	16.40	24.10	19.60	23.00	15.10	8.35	18.60	17.40	13.70	17.20	18.70	27.40
Ho	0.05	2.07	1.38	1.59	0.01	4.67	5.43	6.13	2.93	4.75	3.70	4.60	2.88	1.64	3.58	3.77	2.96	3.69	3.98	6.09
Er	0.15	6.43	3.87	4.35	0.03	14.80	15.90	18.70	8.87	15.20	11.70	14.60	8.31	4.96	11.30	11.70	9.00	11.50	12.40	19.10
Tm	0.03	0.98	0.58	0.72	0.00	2.60	2.76	3.23	1.54	2.81	2.08	2.53	1.39	0.85	2.02	2.11	1.64	2.06	2.17	3.37
Yb	0.11	5.96	3.43	4.67	0.03	16.00	16.80	20.30	10.40	18.50	14.10	16.00	8.70	5.48	12.70	12.90	10.20	12.50	13.40	20.90
Lu	0.02	0.92	0.58	0.72	–[b]	2.59	2.64	3.18	1.52	2.74	1.99	2.31	1.32	0.77	1.88	2.12	1.65	2.08	2.23	3.30
LREE	2.89	102.07	109.79	91.54	0.93	550.77	543.97	643.40	431.67	537.84	455.26	518.60	425.94	264.18	467.44	745.17	511.25	792.56	669.44	518.40
HREE	0.72	34.38	24.83	26.77	0.15	92.45	99.52	116.41	59.47	91.18	73.22	87.84	57.11	31.88	70.21	66.12	52.86	66.31	70.46	104.19
L/H[c]	4.03	2.97	4.42	3.42	6.41	5.96	5.47	5.53	7.26	5.90	6.22	5.90	7.46	8.29	6.66	11.27	9.67	11.95	9.50	4.98
$\sum$REE[c]	3.61	136.44	134.62	118.31	1.07	643.22	643.49	759.81	491.14	629.02	528.48	606.44	483.05	296.06	537.65	811.29	564.11	858.87	739.90	622.59
δCe[c]	0.87	0.47	0.52	0.74	0.71	1.03	1.02	1.04	1.08	1.32	1.25	1.18	0.91	1.70	1.19	3.05	2.72	3.89	3.07	1.23
δEu[c]	0.46	0.48	0.45	0.53	0.90	0.61	0.63	0.65	0.61	0.64	0.64	0.64	0.62	0.65	0.63	0.51	0.55	0.53	0.56	0.58
La_N/Sm_N[c]	5.10	4.04	2.72	2.74	7.79	2.97	2.62	2.59	3.12	3.06	3.12	2.83	3.27	3.30	3.39	7.14	4.64	4.98	4.30	4.45
Gd_N/Yb_N[c]	1.12	0.92	1.67	0.99	0.96	1.16	1.19	1.11	1.16	0.83	0.96	1.05	1.55	1.23	1.08	0.84	0.91	0.94	0.88	0.76
La_N/Yb_N	4.80	3.99	5.86	3.35	7.12	5.10	4.66	4.48	6.18	4.01	4.53	4.59	7.70	5.60	5.47	6.17	5.07	5.00	4.58	4.13

[a] L, T, M, S and A stand for limestone, terra rossa, mixed sample, sedimentary bauxite ore and accumulation bauxite ore, respectively. All the rare earth element values are in ppm.
[b] – Means the content is under the test limit.
[c] L/H represents the concentration ratio of LREE and HREE. $\sum$REE = the sum of La to Lu, $\delta Ce = Ce_N / (La_N \times Pr_N)^{0.5}$, $\delta Eu = Ce_N / (Sm_N \times Gd_N)^{0.5}$, La_N/Sm_N, Gd_N/Yb_N and La_N/Yb_N, where N refers to a chondrite-normalized value.

ND-6	ND-7	ND-8	ND-9	PG3LT-1	PG3LT-2	PG3LT-3	XKC-1	XKC-2	XKC-3	BY-2	BY-3	DJ-3	DJ-4	DJ-5	DJ-6	FS-1	FS-2	FS-3
T	T	T	T	A[a]	A	A	A	A	A	S[a]	S	S	S	S	S	S	S	S
103.00	87.10	77.60	72.40	86.40	210.00	87.90	63.60	74.80	103.00	45.70	54.90	148.00	63.80	42.60	28.40	36.80	92.10	77.50
209.00	185.00	156.00	123.00	131.00	194.00	98.30	179.00	180.00	172.00	422.00	439.00	586.00	302.00	327.00	217.00	277.00	246.00	254.00
18.30	15.90	14.30	13.30	13.10	33.10	14.20	11.10	12.20	15.80	11.30	14.30	39.20	15.20	9.74	7.36	7.30	19.20	16.60
65.50	58.40	53.60	48.50	46.80	121.00	51.40	38.80	44.80	57.50	37.90	48.30	138.00	53.60	34.40	26.50	24.90	63.80	56.70
12.00	11.00	10.30	8.64	9.49	23.00	11.60	8.27	11.10	12.30	8.38	12.30	30.10	12.60	7.42	6.80	5.96	13.80	12.80
2.18	2.05	1.87	1.58	1.70	3.84	2.13	1.71	2.20	2.73	1.15	1.74	4.28	1.94	1.11	0.95	1.17	2.63	2.46
10.50	9.47	9.05	7.62	13.00	26.20	15.30	9.31	11.40	16.20	7.25	10.40	24.30	11.00	7.12	6.71	6.47	11.00	9.76
2.02	1.69	1.68	1.33	4.03	7.76	5.43	2.52	2.85	4.09	1.35	2.18	4.68	2.42	1.37	1.38	1.07	2.47	2.13
12.20	10.80	10.70	7.91	32.30	66.10	46.00	18.80	20.10	30.60	8.08	14.20	27.20	15.20	8.44	8.65	6.33	15.10	12.50
2.63	2.31	2.28	1.70	7.82	15.00	11.10	4.20	4.23	6.75	1.65	2.83	5.47	3.15	1.80	1.80	1.18	2.98	2.25
8.35	7.15	6.90	5.17	24.50	47.60	36.00	13.30	12.90	20.70	5.40	8.88	16.60	10.10	5.69	5.32	4.25	9.13	7.10
1.48	1.26	1.20	0.89	4.20	8.07	6.24	2.39	2.48	3.42	0.94	1.72	3.03	1.91	0.98	0.94	0.78	1.87	1.44
8.96	7.98	7.57	5.52	25.90	52.10	40.40	16.30	15.70	22.00	6.67	12.70	20.00	13.10	6.88	6.16	5.10	14.00	10.00
1.49	1.34	1.23	0.92	4.20	8.58	6.63	2.47	2.67	3.56	1.02	1.87	3.08	1.99	1.01	0.95	0.78	2.13	1.45
409.98	359.45	313.67	267.42	288.49	584.94	265.53	302.48	325.10	363.33	526.43	570.54	945.58	449.14	422.27	287.01	353.13	437.53	420.06
47.63	42.00	40.61	31.05	115.95	231.41	167.10	69.29	72.33	107.32	32.36	54.78	104.36	58.87	33.29	31.91	25.96	58.68	46.63
8.61	8.56	7.72	8.61	2.49	2.53	1.59	4.37	4.49	3.39	16.27	10.42	9.06	7.63	12.68	9.00	13.60	7.46	9.01
457.61	401.45	354.28	298.47	404.44	816.35	432.63	371.77	397.43	470.65	558.79	625.32	1049.94	508.01	455.56	318.92	379.09	496.21	466.69
1.16	1.20	1.13	0.95	0.94	0.56	0.67	1.62	1.43	1.03	4.47	3.77	1.85	2.33	3.86	3.61	4.07	1.41	1.70
0.59	0.61	0.59	0.60	0.47	0.48	0.49	0.60	0.60	0.59	0.45	0.47	0.48	0.50	0.47	0.43	0.58	0.65	0.67
5.40	4.98	4.74	5.27	5.73	5.74	4.77	4.84	4.24	5.27	3.43	2.81	3.09	3.19	3.61	2.63	3.88	4.20	3.81
0.95	0.96	0.96	1.11	0.41	0.41	0.31	0.46	0.59	0.59	0.88	0.66	0.98	0.68	0.84	0.88	1.02	0.63	0.79
7.75	7.36	6.91	8.84	2.25	2.72	1.47	2.63	3.21	3.16	4.62	2.91	4.99	3.28	4.17	3.11	4.86	4.44	5.23

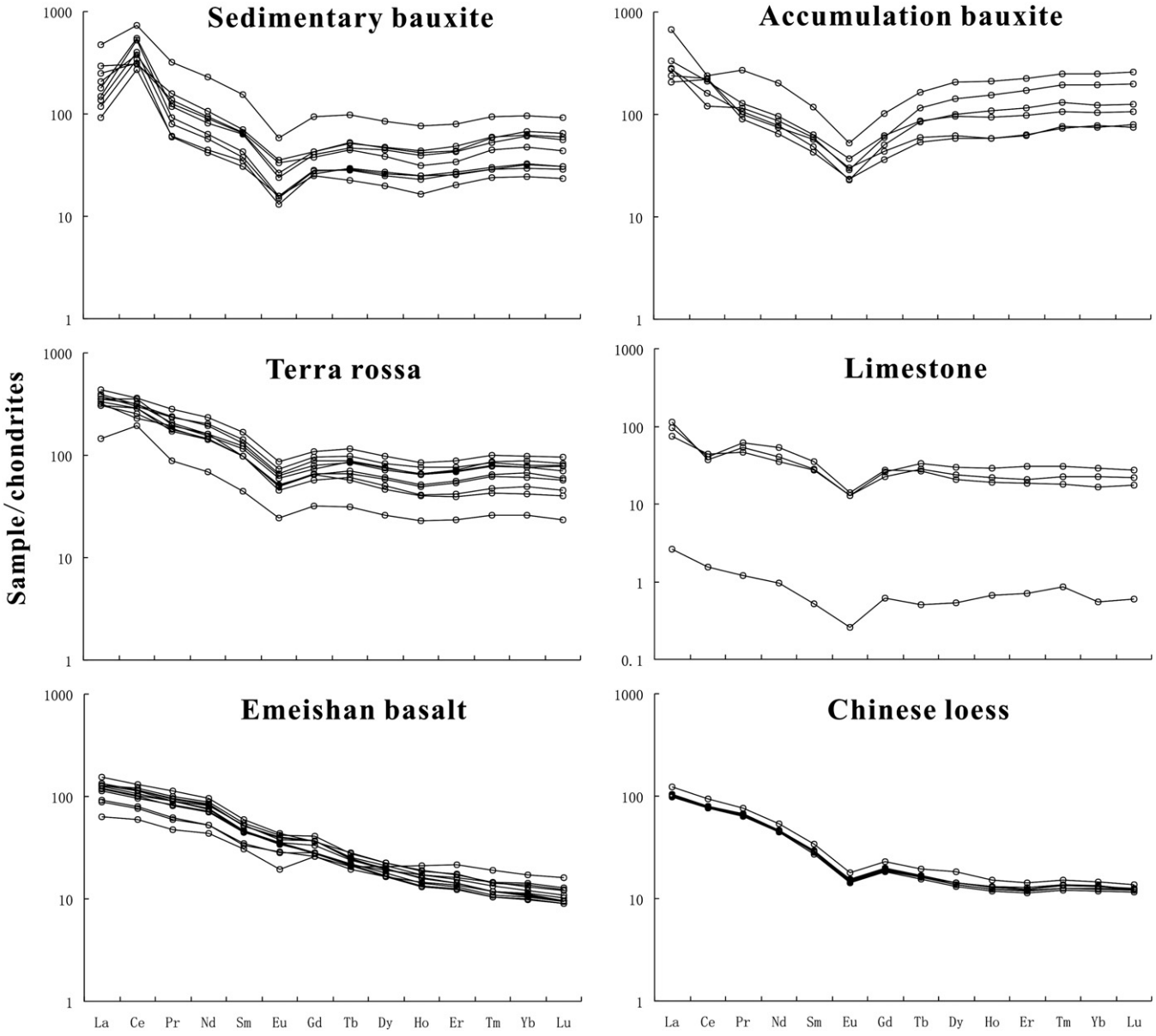

Fig. 8. Chondrite normalized REE spider-diagrams for samples of bauxite deposits, terra rossa, underlying limestone, Emeishan basalt and Chinese loess. The comparative data of the Emeishan basalt cited from Xu (2006) and Zhong et al. (2006), and data of Chinese loess from Ding et al. (2000) and Peucker-Ehrenbrink and Jahn (2001).

the $Fe_2O_3^T/Al_2O_3$ ratios were also considered as an effective provenance indicator (Ji et al., 2004a). The concentration relationships between TiO_2 and Al_2O_3 (Fig. 10A) show that samples of terra rossa and underlying limestone have significant positive correlations ($R^2 = 0.99$), but samples of bauxite deposits have significant negative correlations ($R^2 = 0.82$). The concentration relationships between $Fe_2O_3^T$ and Al_2O_3 (Fig. 10B) display that terra rossa and the underlying limestone have significant positive correlations ($R^2 = 0.99$), and that bauxite deposits present remarkable negative correlations ($R^2 = 0.86$). The significant correlation of TiO_2 vs. Al_2O_3 and $Fe_2O_3^T$ vs. Al_2O_3 in terra rossa and the underlying limestone illustrates that terra rossa is possibly the in situ or quasi-in situ product of the limestone. In contrast, the visible negative correlation in bauxite ores, which is similar to the report of bauxite deposits in Jingxi and Debao Counties, west Guangxi, China (Liu et al., 2012), indicates that they possible have cognate relations.

From Fig. 5, terra rossa has lower CIA values and higher SiO_2 and K_2O contents compared with bauxite deposits. The SiO_2/Al_2O_3 ratios of terra rossa and the underlying carbonate rocks are less variable and consistent (≈ 1), as well as their K_2O/Al_2O_3 ratios (0.02–0.03) (Fig. 11). Furthermore, samples of terra rossa are all concentrated in a small region overlapped by carbonate rock projection zone, but far away from that of the bauxite deposits, UCC, Chinese loess and Emeishan basalt.

Pearce and Cann (1973) stated that some relatively concentrated elements are considered to be immobile elements in the processes of supergene weathering and alteration. Maclean et al. (1997) proposed that it is suitable to use immobile elements to trace the source of aluminium in a particular rock type or unit. The immobile elements were also utilized to address the problem concerning the material sources of sedimentary rocks, terra rossa, loess and deep-sea sediments (MacLean and Kranidiotis, 1987; McLennan, 1989; Muhs and Budahn, 2006; Muhs et al., 2007, Muhs and Budahn, 2009; Olivarez et al., 1991).

However, immobile element is a relative conception, and the mobility of the element may change in different geochemical processes (Little and Lee, 2006; Nesbitt and Markovics, 1997; Raun et al., 1998). In this paper, we used the "plateau points diagram" proposed by Gong et al.

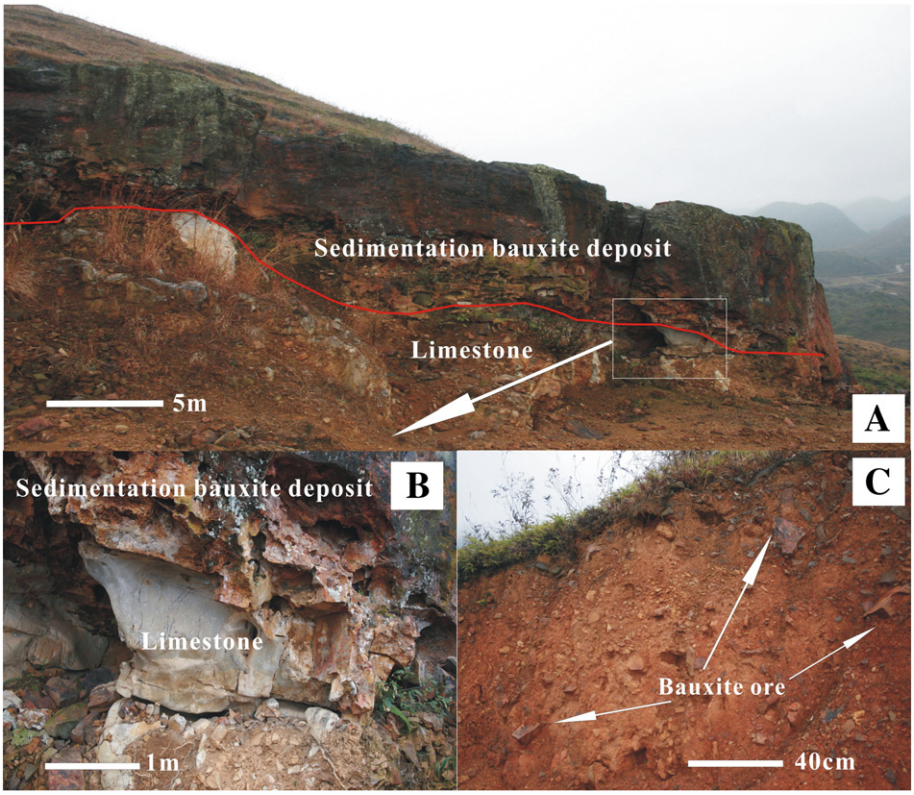

Fig. 9. (A) The parallel unconformity contact relations of sedimentation bauxite deposit and the underlying carbonate rock, (B) the close-up of contact relation of bauxite deposit and underlying limestone, and (C) the brecciaous bauxite ores in thick terra rossa profile.

(2011) to confirm that the Zr, Hf, Ta, Nb, Ti, Th and other trace elements are highly geochemically stable in the processes of laterization, alteration and bauxitization. The plot of Zr/Nb vs. Zr/Hf (Fig. 12A) displays that the Zr/Nb ratios of the samples in the bauxite deposits and terra rossa vary slightly (9–11.9), and the Zr/Hf ratios vary over a wider range (28.8–37.7). Moreover, the Zr/Nb ratios of carbonate rocks have a little variation (9.19–15.52) that are quite close to that of the bauxite deposits and terra rossa (9–11.9), whereas the Zr/Hf ratios of them change significantly (29.15–47.60). There is a great deal of overlap in samples of bauxite deposits and terra rossa, which are nearby the UCC and far away from the field occupied by the samples of Chinese loess and Emeishan basalt. However, in the diagram of Nb/Hf vs. Zr/Ta ratios (Fig. 12B), the projected points of samples of bauxite deposits and terra rossa and composite samples almost overlap with each other, and the regions defined by the samples of carbonate rock, Chinese loess and Emeishan basalt are near them.

Hallberg (1984) proposed that the Zr/Ti ratio provided much chemical information about the provenance. Floyd and Winchester (1978) utilized the Zr/TiO_2 vs. Nb/Y diagram to determine the parent rock of the laterite. Likewise, we chose the Zr/TiO_2 vs. Nb/Y diagram to constrain the material sources of bauxite deposits (Fig. 12C). All samples have no significant variations of Zr/TiO_2 ratios, except for Emeishan basalt samples that have lower values. Regions occupied by samples of the two types of typical bauxite deposits are close to each other, and a few samples of terra rossa fall within the area defined by the Chinese loess samples.

5.1.4. Evidences from REE parameters

Most REE parameters (δCe and δEu) and the ratios (La_N/Yb_N, La_N/Sm_N and Gd_N/Yb_N) of rare earth elements were proposed to reflect the source and evolution trend of sediments (Ji et al., 2004b; Muhs et al., 2007). Plots of La_N/Yb_N vs. δEu and Gd_N/Yb_N vs. δEu are widely utilized to constrain the origin of eolian dust in deep-sea sediments, and reveal the sources of loess, soils and other sedimentation rocks and sediments (Ji et al., 2004b; McLennan, 1989; Muhs and Budahn, 2006; Muhs et al., 2007); Nakai et al., 1993; Sun, 2002.

The plot of La_N/Yb_N vs. δEu (Fig. 13A) shows that the Eu values of bauxite deposits, terra rossa, the underlying carbonate rocks and Chinese loess range from 0.43 to 0.67, but theδEu values of Emeishan basalt samples (ranging from 0.86 to 0.98) are distinctly higher than those of the other samples. Furthermore, theδEu values of terra rossa, Chinese loess and the UCC (refer to the upper continental crust) vary over a small range, close to the value of 0.65. The La_N/Yb_N ratios of terra rossa samples vary over a large range (from 4.01 to 8.84), some of which (profile PG-2) fall within the field defined by the sedimentation bauxite deposits, and the rest of which (profile ND) fall within the region occupied by samples of Chinese loess. The carbonate rock samples mainly fall within the region of sedimentation bauxite deposits, and samples of accumulation bauxite deposit with lower La_N/Yb_N values (1.47–3.21) are located on the left near this region. The diagram of Gd_N/Yb_N vs. δEu indicates that bauxite deposits, terra rossa and the underlying carbonate rocks (except for samples DJ-1 and PG2-9) are concentrated together and are separated from Chinese loess, Emeishan basalt and the UCC by the Gd_N/Yb_N ratio value of 1.31(Fig. 13B).

5.1.5. Discussion about the possible source

The geochemical tracer methods discussed above show that two types of bauxite deposits were possibly derived from an identical material source. However, the differences between them in geochemical and geological characteristics indicate that accumulation bauxite deposit might be transformed from primary sedimentation bauxite deposit by long period crushing, weathering and leaching. Although it is hard to make sure whether the eolian source similar to Chinese loess and volcanic rock related to Emeishan basalt is the material source of bauxite deposits in western Guangxi, the study results do not support that the two components are the major material genesis.

The underlying Permian limestone significantly contributes to the material source of terra rossa according to the geochemical and

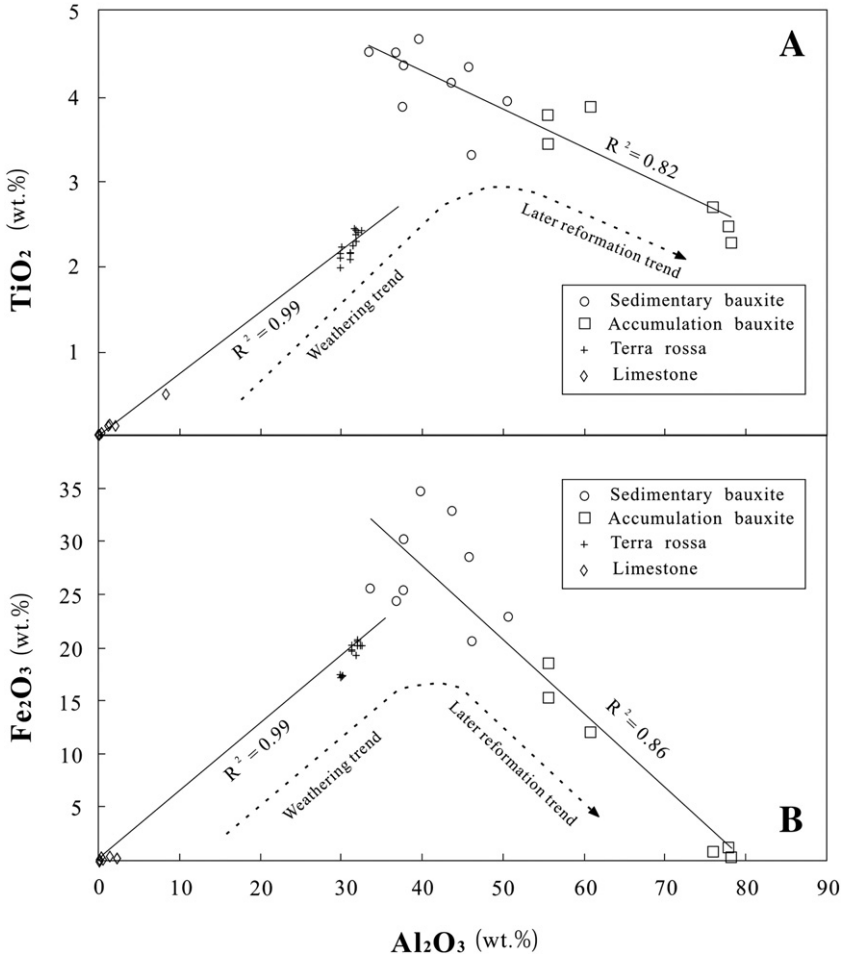

Fig. 10. (A) Distribution of TiO_2 and Al_2O_3 in bulk samples from western Guangxi. (B) Distribution of $Fe_2O_3^T$ and Al_2O_3 in bulk samples from western Guangxi. See the text for detailed explanation.

geomorphology evidences. The geochemical tracer method shows that there is a quite close affinity among terra rossa, bauxite deposits and the underling limestone, which indicates that terra rossa and bauxite deposits possibly have similar or identical material source. Moreover, geological and geochemical evidences also support that this material source might be a kind of Permian carbonate rock similar to the

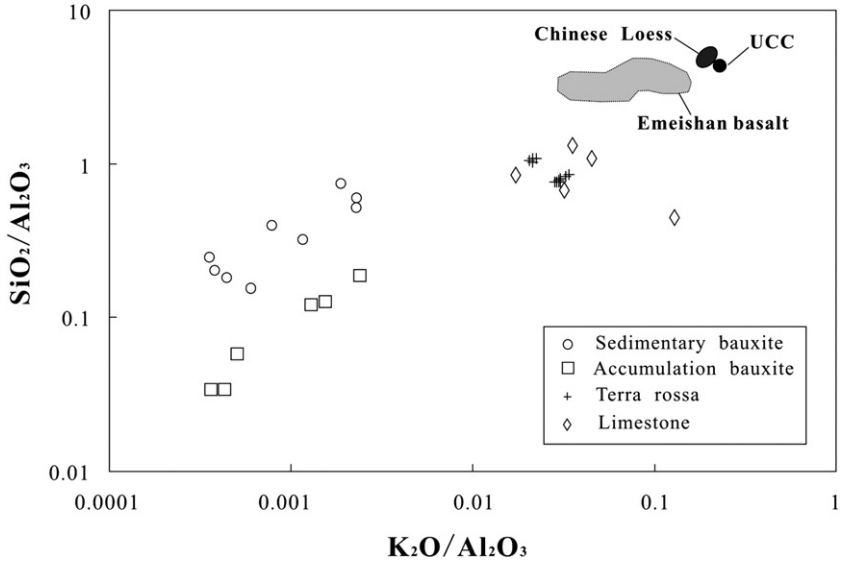

Fig. 11. Plot of SiO_2/Al_2O_3 vs. K_2O/Al_2O_3 for bulk samples in western Guangxi comparing with UCC, Chinese loess and Emeishan basalt. Upper continental crust (UCC) data cited from Taylor and McLennan (1985) represent detrital component, Chinese loess values (after Ding et al. 2000 and Peucker-Ehrenbrink and Jahn, 2001) represent eolian material source (Ding et al., 2000; Liu, 1985; Sun, 2002), and Emeishan basalt data used here from Xu (2006) and Zhong et al. (2006) stand for igneous rock genesis.

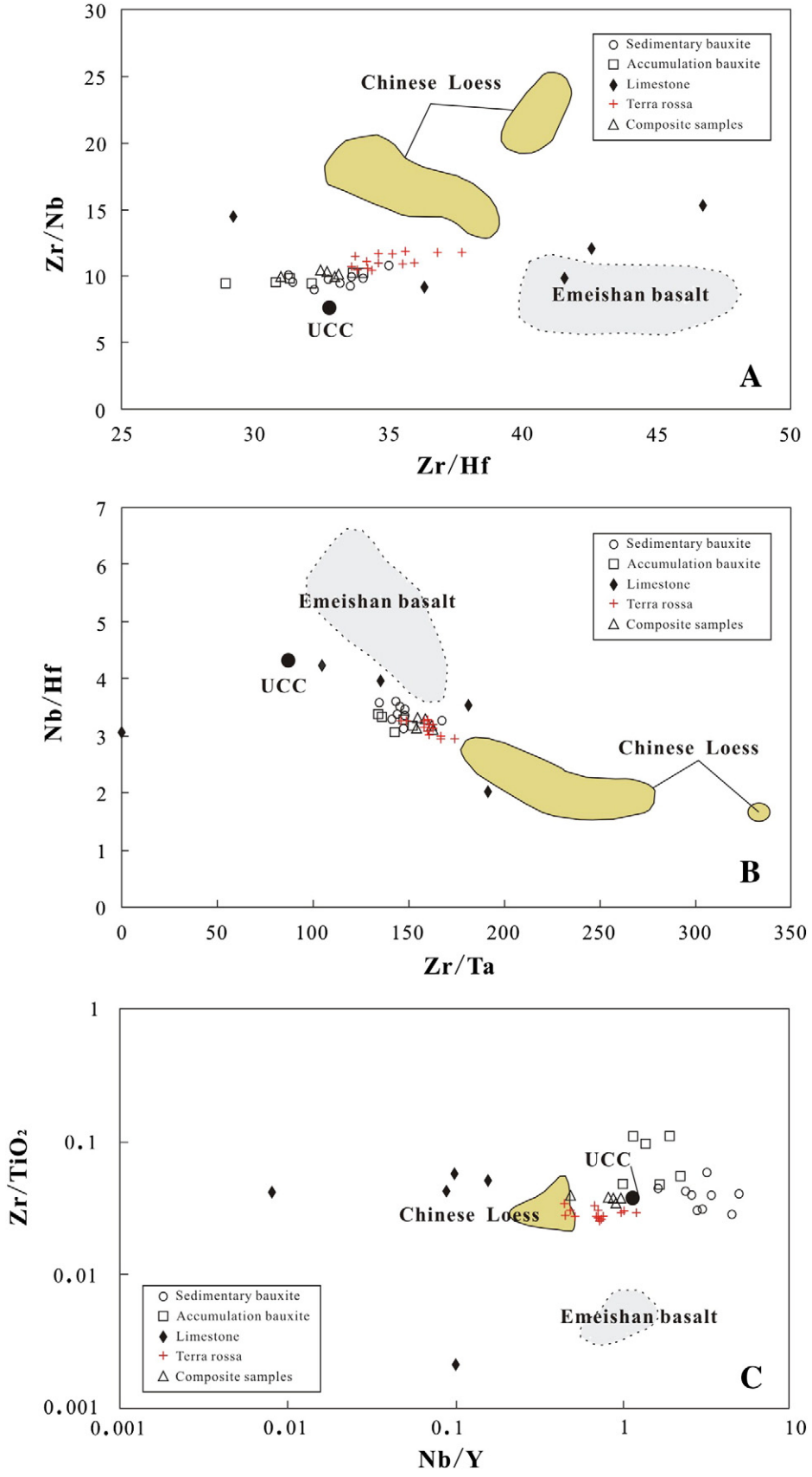

Fig. 12. (A) Zr/Nb vs. Zr/Hf, (B) Nb/Hf vs. Zr/Ta, and (C) Zr/TiO_2 vs. Nb/Y diagrams of bulk samples in western Guangxi comparing with UCC, Chinese loess and Emeishan basalt. The Emeishan basalt, Chinese loess and UCC data are of the same derivation as shown in Fig. 11.

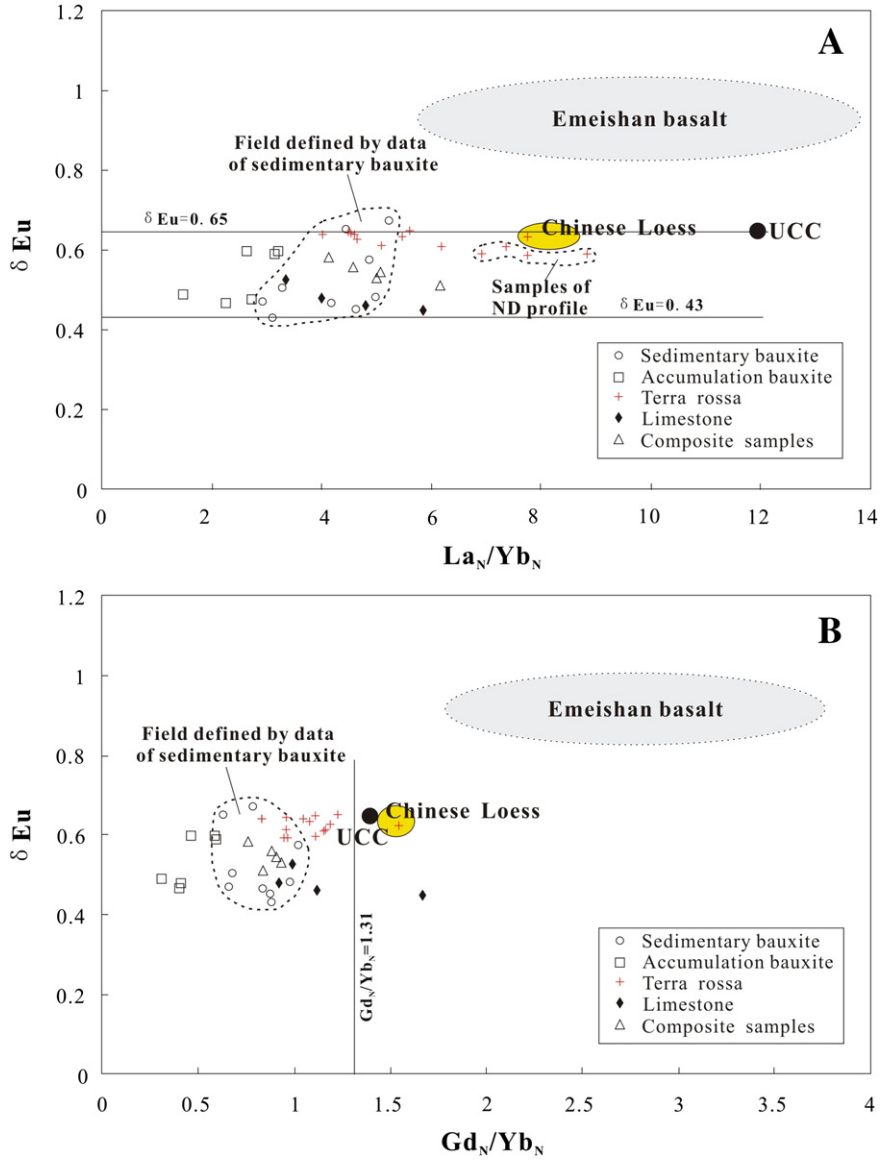

Fig. 13. (A) La_N/Yb_N vs. δEu and (B) Gd_N/Yb_N vs. δEu plots for bauxite deposits, terra rossa and underlying limestone in western Guangxi comparing with the potential genesis. Explanations are shown in the box. The Emeishan basalt, Chinese loess and UCC data derive from the same derivation as shown in Fig. 11.

underlying limestone. However, it can not rule out the possibilities of input of other genesis.

5.2. Element geochemical behaviors in the pedogenesis and diagenesis processes

The former discussions and conclusions have confirmed the succession of bauxite deposits, terra rossa and the underlying limestone. Subsequently, we attempt to figure out the formation and evolution process of bauxite deposits in western Guangxi via the study of various element geochemical behaviors in the pedogenesis and diagenesis processes. The end member of parent rock is substituted by the underlying Permian limestone, and terra rossa represents the detrital component or paleo-weathering product. Composite samples are the mixture of terra rossa and accumulation bauxite ores which shows that all composite samples are located in the region between terra rossa and accumulation bauxite deposit end members (Figs. 12–15).

5.2.1. Major element geochemical behaviors

In the transformation from limestone to terra rossa, the contents of less mobile elements, such as Al, Fe, Ti, and Si, increased (Figs. 10 and 14), and the concentrations of the mobile element Na decreased, but the contents of K remained unchanged (Fig. 14A). Calcite and dolomite in the parent rocks (referring to carbonate rocks) were rapidly dissolved and removed, leading to the migration of Ca and Mg and relative accumulation of less mobile elements. The element with low ionic potential, such as Na, is easier to remain in solution during weathering process. However, K which has a large ionic radius is preferentially adsorbed on clay minerals according to the cation exchange capacity theory (Panahi et al., 2000). It might be a reason why K content did not decrease rapidly and largely. Another probable cause is that the K-bearing mineral, such as illite, still preserved in weathering remnants.

The formation of primary bauxite deposit is actually the result of deeply weathering and complicated geological mineralization. This process is characterized by enrichment of Al, Fe, and Ti, significant depletion of Si and K, and slight depletion of Na, Ca, and Mg (Figs. 5, 10 and 14). The concentrations of Na, Ca and Mg from samples of sedimentation bauxite deposit are similar to those of terra rossa, because they have almost leached out in previous process. Under long-period eluviation, a large number of K adsorbed on the surface of clay minerals were released, and K-bearing minerals were decomposed. Meanwhile, clay

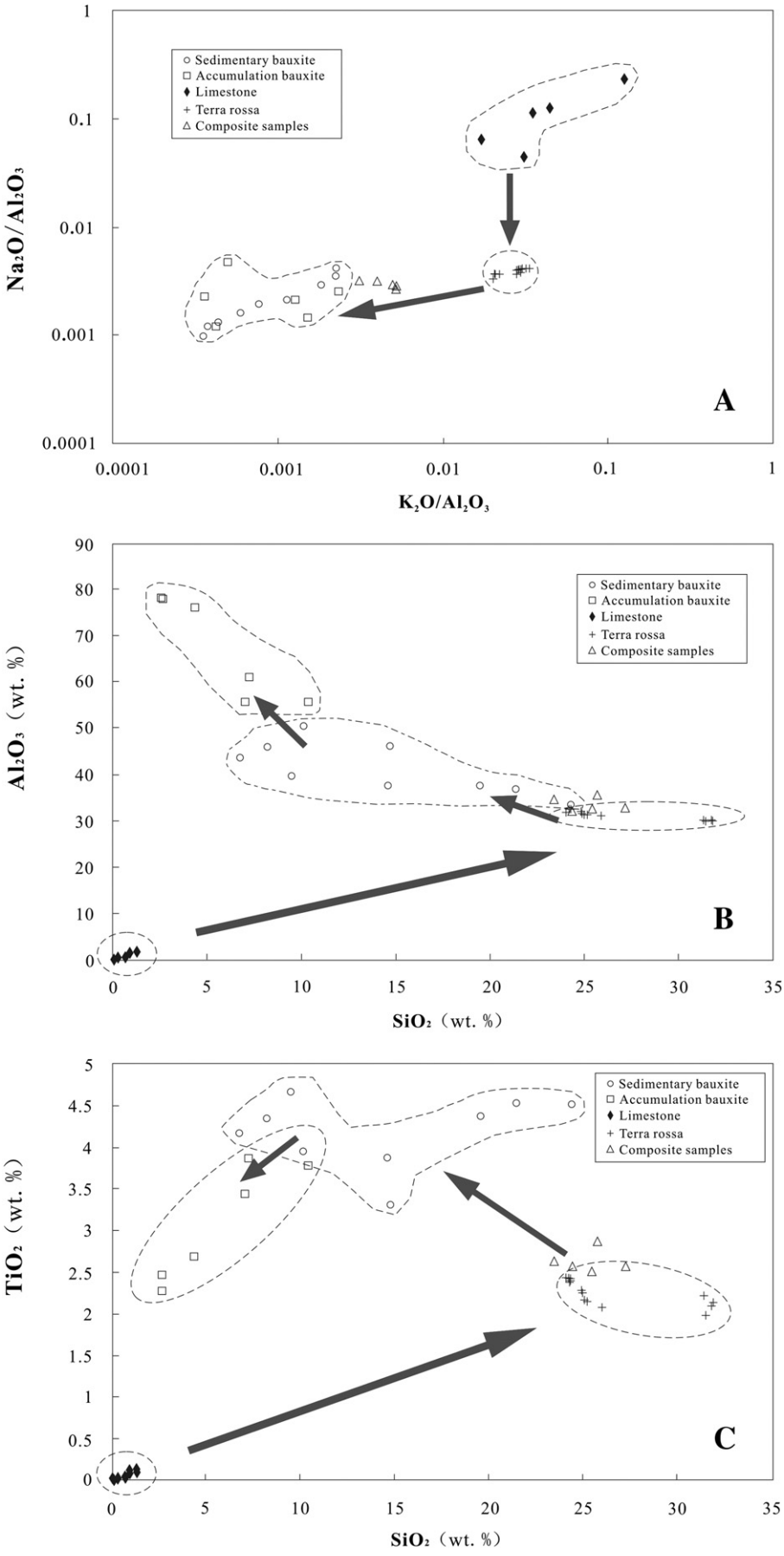

Fig. 14. (A) Na_2O/Al_2O_3 vs. K_2O/Al_2O_3, (B) Al_2O_3 vs. SiO_2 and (C) TiO_2 vs. SiO_2diagrams of bulk samples in western Guangxi.

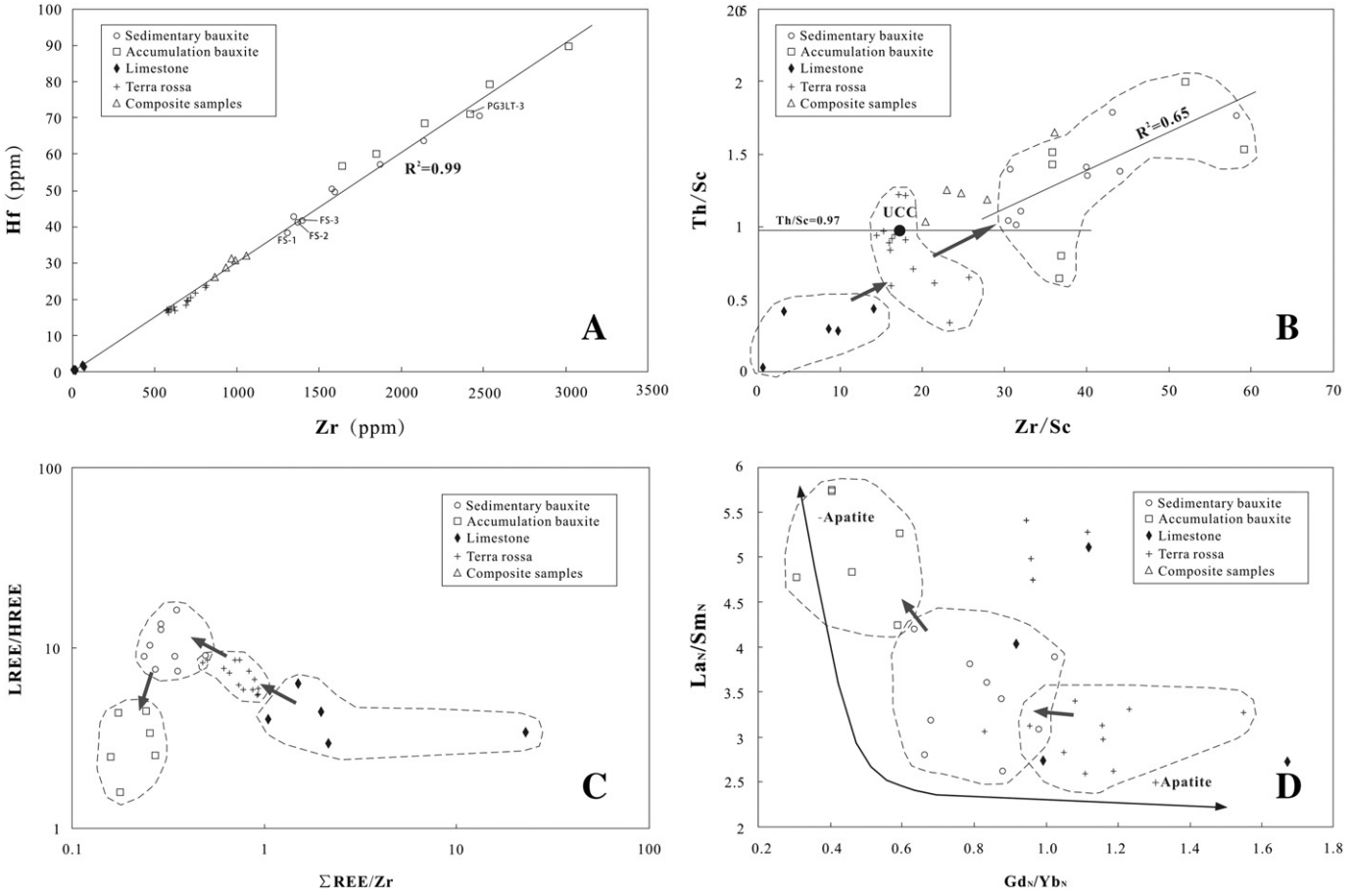

Fig. 15. (A) Hf vs. Zr concentrations, (B) Th/Sc vs. Zr/Sc ratios, (C) LREE/HREE vs. ∑REE/Zr ratios and (D) La_N/Sm_N vs. Gd_N/Yb_N ratios for bulk samples in western Guangxi.

minerals (such as kaolinite and illite) transformed into gibbsite under strong weathering, and then became diasporite in the diagenesis and bauxitization process. The SiO_2/Al_2O_3 and K_2O/Al_2O_3 ratios in samples of the sedimentation and accumulation type bauxite deposits have significant positive correlations (0.77 and 0.99, respectively) (Fig. 11), which illustrates that K of bauxite deposits mainly existed in the phyllosilicate minerals, such as muscovite, biotite, illite and chlorite (Liu et al., 2012).

During the process from sedimentation-type to accumulation-type bauxite deposit, the later reconstruction led to depletion of Fe and Ti in accumulation bauxite deposit, especially the samples from profile PG3LT (Fig. 10). The concentration of Al increased, but that of mobile elements had dropped to an extremely low level. Generally, the solubility of iron is related to oxidation–reduction and pH value, but it is not the case for Al and Ti whose solubility is controlled mainly by environmental pH value (Ji et al., 2004a). Pyrite in the roof and floor of primary bauxite deposit was rapidly oxidized in the supergene environment. The vitriolic acid released from oxidized pyrite would drastically reduce the pH value of oxidization-zone environment (Liu et al., 2004b). They formed $Fe(SO_4)$ and $Fe_2(SO_4)_3$ in the strongly acidic supergene environment ($pH \approx 2$). In addition, the convenient drainage increased the transportation capacity of Fe, and the element Fe almost completely migrated from the bauxite ores (Liu et al., 1984). The element Fe that leached out of the bauxite ore was deposited with increasing pH in the surroundings (decomposing of feldspar and the underlying carbonate rock could neutralize the acid). It was not until the pH value reached 4 to 5 that the element Fe began to be transformed into hematite and goethite. In the field, the ferricrete is frequently found at the bottom of the accumulation bauxite deposit zone (Fig. 3). The elements Ti and Al are generally immobile in the supergene environment. However, the mobility of Al could increase in the strongly acidic ($pH \leq 4$) or strongly alkaline environment ($pH \geq 10$), and, similarly, the element Ti could steadily exist in the strongly acidic solution ($pH \leq 2$) (Liu et al., 1984). In this transformation process, the contents of TiO_2 decreased, which was possibly associated with the regional strongly acidic environment caused by the oxidation of pyrite.

5.2.2. Trace element geochemical behaviors

In the parent rocks, trace elements are distributed between rock-forming and accessory minerals. The rock-forming minerals may be dissolved during weathering, whereas the accessory minerals are commonly resistant to weathering. Therefore, the distribution between these two groups determines the weathering characteristics of elements (Bardossy and Aleva, 1990; Mordberg, 1996). The elements Zr and Hf are extremely stable in the process of supergene weathering, because they generally exist in zircon which has strong weathering resistance (Milnes and Fitzpatrick, 1989). The element Sc, which is related with Fe during the weathering process, remains relatively low in concentrations in natural waters and is mainly concentrated in clay minerals of soil (Cullers, 1988; Dennen and Anderson, 1962; Liu et al., 1984). The Zr/Sc ratio therefore is used as a tracer for zircon or heavy mineral concentrations and it was generally accepted that the elements Sc and Th are transferred quantitatively from the source to the host sediments, and consequently, the Th/Sc ratio is generally used to reflect the bulk source composition (Alvarez and Roser, 2007; McLennan, 1989; McLennan and Taylor, 1991; Taylor and McLennan, 1985).

The concentration plot of Zr vs. Hf (Fig. 15A) displays that bauxite deposits, terra rossa and the underlying carbonate rocks, as well as composite samples, all fall in a line which passes through the origin ($R^2 = 0.99$). It indicates that they have the cognate genesis. From

limestone to terra rossa to bauxite deposits, the concentrations of Zr and Hf kept rising with increasing weathering degree, which illustrates that the elements Zr and Hf are highly stable in the process of supergene weathering. Overall, the covariance and immobility of the elements Zr and Hf imply that they may principally exist in zircon.

The Th/Sc ratios in bauxite deposit samples are predominately higher than those of UCC, and those in most of terra rossa samples are lower than 0.97. As for the samples of underlying carbonate rocks, the Th/Sc ratios are lower than 0.5 (Fig. 15B). The process from limestone to terra rossa to bauxite deposit is similar to the weathering trend of dolomite weathered crust described by Ji et al. (2004a). The Th/Sc and Zr/Sc ratios in sedimentation bauxite deposit have a positive correlation ($R^2 = 0.65$) (Fig. 15B), which illustrates that Th, Zr and Sc in bauxite deposit samples mainly preserved in immobile heavy minerals.

5.2.3. REE geochemical behaviors

It is generally believed that the rare earth elements primarily exist in the following three fractions in carbonate rocks: (I) the detritus fraction, which was composed chiefly of stable REE independent minerals, (II) the absorbed fraction, which was in the form of ions absorbed on clay minerals, such as montmorillonite and kaolinite, or hydroxides of iron and manganese and other metals (Aagard, 1974; Parekh et al., 1977; Roaldset, 1973, 1979), and (III) the authigenic carbonate and phosphate fraction, which was formed in the sedimentation and diagenetic processes. The latter two forms are the main fractions hosting REEs (Balashov and Girin, 1969; Ji et al., 2004b; Johannesson and Zhou, 1997; Mameli et al., 2007). Under the mild and humid conditions, intensive chemical weathering makes the REEs become mobile (Balashov et al., 1964), while REE fractionation in the weathering profile is controlled by environmental factors such as Eh, pH and drainage condition and the stability of secondary REE-bearing minerals (Aubert et al., 2001; Braun et al., 1998; Caspari et al., 2006; Laveuf and Cornu, 2009; Mongelli, 1993).

As viewed from Fig. 15C, the $\sum$REE/Zr ratios of bauxite deposits, terra rossa and the underlying limestone show a declined tendency with increased weathering maturity. However, LREE/HREE ratio displays such a tendency as to increase first and then decrease. It indicates that the evolution process from limestone to bauxite deposits was characterized by leaching and removal of total REE and the weathering system preferentially leached and removed HREE, and concentrated LREE relatively. Many authors addressed the same finding with the reason that HREE cations possess higher ionic potential than LREE cations, which means HREE cations easily combined with $(CO_3)^{2-}$, $(SO_4)^{2-}$, $(NO_3)^{-}$ and $(SiO_4)^{4-}$ to form stable complex ions. Therefore, the stability of HREE is rising in aqueous solution (Cantrell and Byrne, 1987; Smedley, 1991). However, when pH $\leq$ 6, REE occurs primarily as free ions (Smedley, 1991; Turner et al., 1981; Wood, 1990), i.e. the complexation capacity is less prevalent. That is because, in acidic environment, HREE is more adsorbed than LREE in the same trivalent state, according to the lanthanide contraction. In the later reconstruction stage, long-term intensive supergene chemical weathering and strongly acidic environment led to the decline of LREE/HREE.

Laboratory-based studies showed that REEs were trapped into the apatite structure quickly (Watson and Green, 1981), so that apatite partially controlled the fractionation of REEs from soil solutions (Laveuf and Cornu, 2009). The diagram of La_N/Sm_N vs. Gd_N/Yb_N ratios (Fig. 15D) displays a variation trend of apatite in the weathering process (Ji et al., 2004b; Savoy et al., 2000). Most samples distribute along the variation trend curve of apatite, and samples of terra rossa and limestone overlapped together (Fig. 15D). It illustrates that in the evolution process from terra rossa to bauxite deposits, the weathering, pedogenesis, diagenesis, and later reformation play a significant role in the destruction of apatite. However, from limestone to terra rossa, the leaching is useless for the decomposition of apatite. Many reports also propose the similar view that in highly weathered materials secondary phosphates disappear (Laveuf and Cornu, 2009; Taunton et al., 2000).

6. Conclusions

Major, rare earth and trace element data indicates that the sedimentation and accumulation type bauxite deposits have identical material source and close affinity with terra rossa and underlying limestone. The carbonate rocks similar to the underlying limestone possibly are the major material source of bauxite deposits and terra rossa in western Guangxi. The comparison result of the relevant data of UCC, Chinese loess and Emeishan basalt samples shows that these end members possibly made limited contributions to the source material of bauxite deposits.

During the process of pedogenesis, the mobile elements, such as Ca, Mg and Na, were preferentially dissolved and emigrated from parent rocks, which led to the relative accumulation of immobile elements, such as Al, Fe, Ti and Si. However, in the bauxitization and diagenesis stage, elements K and Si were removed from the system. In the later reconstruction stage, the strongly acidic environment caused by decomposition of pyrite increased the activities of many elements, including several “insolvable” elements (e.g. elements Fe and Ti). The activities of most trace elements are controlled by the stabilities of their carrier minerals. For example, the trace elements Hf, Zr, Th and Sc presented good stabilities in supergene weathering, which is attributed to the emergence of zircon. The result also shows that the total concentrations of REE decreased normalized by zirconium in the evolution process, and the migration of HREE and relative enrichment of LREE dominated the pedogenesis and bauxitization stages. However, in the later reconstruction, the strongly acidic environment was beneficial to enrichment of HREE relative to LREE.

Acknowledgments

We appreciate Prof. D. Liang for the fieldwork and M. Liu and JY Cui for main and trace element analysis, respectively. Furthermore, we are indebted to Prof. ZW Zhang for discussions and suggestions about this study. This work was jointly supported by the Hundred Talents Program of Chinese Academy of Sciences, the National Natural Science Foundation of China (NSFC) grant (Nos. 41073096 and 40473051) and the National Key Basic Research Program of China (2013CB956702).

References

Aagard, P., 1974. Rare earth elements adsorption on clay minerals. Bulletin du Groupe Francais des Argiles 26, 193–199.
Alvarez, N.O.C., Roser, B.P., 2007. Geochemistry of black shales from the Lower Cretaceous Paja Formation, Eastern Cordillera, Colombia: source weathering, provenance and tectonic setting. Journal of South American Earth Sciences 23, 271–289.
Aubert, D., Stille, P., Probst, A., 2001. REE fractionation during granite weathering and removal by waters and suspended loads: Sr and Nd isotopic evidence. Geochimica et Cosmochimica Acta 65, 387–406.
Balashov, Y.A., Girin, Y.P., 1969. On the reserve of mobile rare earth elements in sediment rocks. Geochemistry International 7, 649–658.
Balashov, Y.A., Ronov, A.B., Migdisov, A.A., Turanskays, N.V., 1964. The effects of climate and facies environment on the fractionation of rare earths during sedimentation. Geochemistry International 1, 951–969.
Banerjee, A., Merino, E., 2011. Terra rossa genesis by clay-for-limestone replacement: part III, dynamic quantitative model and test of the replacement mechanism. Journal of Geology 119, 259–274.
Bardossy, G., 1982. Karst Bauxites. Elsevier, Amsterdam (441 pp.).
Bardossy, G., Aleva, G.J.J., 1990. Lateritic Bauxite. Elsevier, Amsterdam (624 pp.).
Braun, J.-J., Viers, J., Dupre, B., Polve, M., Ndam, J., Muller, J.-P., 1998. Solid/liquid REE fractionation in the lateritic system of Goyoum, East Cameroon: the implication for the present dynamics of the soil covers of the humid tropical regions. Geochimica et Cosmochimica Acta 62, 273–299.
Brimhall, G.H., Lewis, C.J., Ague, J.J., Dietrich, W.E., Hampel, J., Teague, T., Rix, P., 1988. Metal enrichment in bauxites by deposition of chemically mature Aeolian dust. Nature 333, 819–824.
Calagari, A.A., Abedini, A., 2007. Geochemical investigations on Permo-Triassic bauxitehorizon at Kanisheeteh, east of Bukan, West-Azarbaidjan, Iran. Journal of Geochemical Exploration 94, 1–18.
Cantrell, K.J., Byrne, R.H., 1987. Rare earth element complexation by carbonate and oxalate ions. Geochimica et Cosmochimica Acta 51 (3), 597–605.
Caspari, T., Bäumler, R., Norbu, C., Tshering, K., Baillie, I., 2006. Geochemical investigation of soils developed in different lithologies in Bhutan, Eastern Himalayas. Geoderma 136, 436–458.

Chen, Q., Lan, W., 1991. A study on the genesis of the Permian bauxite deposit at Pingguo, Guangxi. Geology of Guangxi 4, 43–49 (in Chinese with English abstract).
Cullers, R.L., 1988. Mineralogical and chemical changes of the soil and stream sediment formed by intensive weathering of the Danburg granite, Georgia, USA. Lithos 21, 301–314.
Deng, J., Wang, Q.F., Yang, S.J., Liu, X.F., Zhang, Q.A., Yang, L.Q., Yang, Y.H., 2010. Genetic relationship between the Emeishan plume and the bauxite deposits in western Guangxi, China: constraints from U–Pb and Lu–Hf isotopes of the detrital zircons in bauxite ores. Journal of Asian Earth Sciences 37, 412–424.
Dennen, W.H., Anderson, P.J., 1962. Chemical changes in incipient rock weathering. Geological Society of America Bulletin 73, 357–383.
Ding, Z.L., Sun, J.M., Yang, S.L., Liu, T.S., 2000. Geochemistry of the Pliocene red clay formation in Chinese Loess Plateau and implications for its origin, source provenance and paleoclimate change. Geochimican et Cosmochimica Acta 65, 901–913.
Durn, G., 2003. Terra rossa in the Mediterranean region: parent materials, composition and origin. Geologia Croatica 56 (1), 83–100.
Esmaily, D., Rahimpur-Bonab, H., Esna-Ashari, A., Kananian, A., 2009. Petrography and geochemistry of the Jajram karst bauxite ore deposits, NE Iran: implications for source rock material and ore genesis. Turkish Journal of Earth Sciences 1, 31.
Feng, J.L., Gao, S.P., Zhang, J.F., 2011. Lanthanide tetrad effect in ferromanganese concretions and terra rossa overlying dolomite during weathering. Chemie der Erde-Geochemistry 71 (4), 349–362.
Floyd, P.A., Winchester, J.A., 1978. Identification and discrimination of altered and metamorphosed volcanic rocks using immobile chemical elements. Chemical Geology 21, 291–306.
Galović, E.k, Ilijanić, N., Peh, Z., Miko, S., Hasan, O., 2012. Geochemical discrimination of Early Palaeogene bauxites in Croatia. Geologia Croatica 04 (65/1), 53–65.
Gong, Q.J., Deng, J., Yang, L.Q., Zhang, J., Wang, Q.F., Zhang, G.X., 2011. Behavior of major and trace elements during weathering of sericite–quartz schist. Journal of Asian Earth Sciences 42, 1–13.
Hallberg, J.A., 1984. A geochemical aid to igneous rocks type identification in deeply weathered terrain. Journal of Geochemical Exploration 20, 1–8.
Ji, H.B., Wang, S.J., Ouyang, Z.Y., Zhang, S., Sun, C.X., Liu, X.M., Zhou, D.Q., 2004a. Geochemistry of red residua underlying dolomites in karst terrains of Yunnan–Guizhou Plateau: I. The formation of the Pingba profile. Chemical Geology 203, 1–27.
Ji, H.B., Wang, S.J., Ouyang, Z.Y., Zhang, S., Sun, C.X., Liu, X.M., Zhou, D.Q., 2004b. Geochemistry of red residua underlying dolomites in karst terrains of Yunnan–Guizhou Plateau: II. The mobility of rare earth elements during weathering. Chemical Geology 203, 29–50.
Johannesson, K.H., Zhou, X.P., 1997. Geochemistry of the rare earth elements in natural teroterrial waters: a review of what is currently known. Chinese Journal of Geochemisty. 16 (1), 20–42.
Karadağ, M.M., Küpeli, S., Arýk, F., Ayhan, A., Zedef, V., Döyen, A., 2009. Rare earth element (REE) geochemistry and genetic implications of the Mortas-bauxite deposit (Seydis-ehir/Konya—Southern Turkey). Chemie der Erde-Geochemistry 69, 143–159.
Laveuf, C., Cornu, S., 2009. A review on the potentiality of rare earth elements to trace pedogenetic processes. Geoderma 154, 1–12.
Li, J.Y., Zhu, L.J., 2004. On modern weathering crust and palaeo-weathering crust of carbonate rock. Carsologica Sinica 23 (1), 56–62 (in Chinese with English abstract).
Li, J.Y., Wang, C.F., Fan, T.Z., 1991. Weathering crust of carbonate rocks and process of karst earth formation. Carsologica sinica 10 (1), 29–38 (in Chinese with English abstract).
Li, J.Y., Wang, C.F., Fan, T.Z., Zhu, L.J., Chen, J., 1995. The characteristics of structure and texture of residual laterite and their genesis. Carsologica sinica 14 (1), 31–39 (in Chinese with English abstract).
Li, J.Y., Zhu, L.J., Liang, F., Chen, J., 2002. Study with scanning electron microscope on micro-texture of the residual red clay from carbonate rocks. Carsologica sinica 21 (4), 233–237 (in Chinese with English abstract).
Little, M.G., Lee, A.C.T., 2006. On the formation of an inverted weathering profile on Mount Kilimanjaro, Tanzania: Buried paleosol or groundwater weathering? Chemical Geology 235 (3–4), 205–221.
Liu, T.S., 1985. Loesses and the Environment. Science in China Press, Beijing 481.
Liu, C.L., Qin, Z.A., 1991. Geochemistry of trace elements in bauxite of China. Acta Sedimentologica Sinica 9 (2), 112–116 (in Chinese with English abstract).
Liu, Y.J., Cao, L.M., Li, Z.L., Wang, H.N., Chu, T.Q., Zhang, J.R., 1984. Element Geochemistry. Science Press 1–548 (Chinese book).
Liu, X.M., Wang, S.J., Feng, Z.G., Sun, C.X., 2004a. Identification of origin of limestone soil—case study of profiles in central and north Guizhou. Soils 36 (1), 30–36 (in Chinese with English abstract).
Liu, Y.H., Mao, X.D., Huang, T.X., 2004b. Metallogenic mechanism of gibbsite from accumulated bauxite in western Guangxi province. Journal of Earth Sciences and Environment 26 (2), 26–31.
Liu, X.F., Wang, Q.F., Deng, J., Zhang, Q.Z., Sun, S.L., Meng, J.Y., 2010. Mineralogical and geochemical investigations of the Dajia Salento-type bauxite deposits, western Guangxi, China. Journal of Asian Earth Sciences 105, 137–152.
Liu, X.F., Wang, Q.F., Zhang, Q.Z., Feng, Y.W., Cai, S.H., 2012. Mineralogical characteristics of the superlarge Quaternary bauxite deposits in Jingxi and Debao counties, western Guangxi, China. Journal of Asian Earth Sciences 52, 53–62.
Lucke, B., 2007. Demise of the Decapolis: Past and Present Desertification in the Context of Soil Development, Land Use, and Climate: Saarbrücken. VDM, Germany (http://opus.kobv.de/btu/volltexte/2007/343/).
Lucke, B., Kemnitz, H., Bäumler, R., 2012. Boletín De La Sociedad Geológica Mexicana 64 (1), 21–35.
Lyew-Ayee, P.A., 1986. A case for the volcanic origin of Jamaican bauxites. Proceedings of the VI Bauxite Symposium 1986. Journal of the Geological Society 1, 9–39.
MacLean, W.H., Kranidiotis, P., 1987. Immobile elements as monitors of mass transfer in hydrothermal alteration: Phelps Dodge massive sulfide deposit. Matagami. Quebec. Economical Geology 82, 951–962.
MacLean, W.H., Bonavia, F.F., Sanna, G., 1997. Argillite debris converted to bauxite during karst weathering: evidence from immobile element geochemistry at the Olmedo Deposit, Sardinia. Mineralium Deposita 32 (6), 607–616.
Mameli, P., Mongelli, G., Oggiano, G., Dinelli, E., 2007. Geological, geochemical and mineralogical features of some bauxite deposits from Nurra (Western Sardinia, Italy): insights on conditions of formation and parental affinity. International Journal of Earth Sciences 96, 887–902.
Marker, A., de Oliveira, J.J., 1994. Trace Element Distributions in Brazilian Cerrado Soils at the Landscape and Micrometer Scale. Thesis of the Purdue University, West Lafayett (173 pp.).
McLennan, S.M., 1989. Rare earth elements in sedimentary rocks influence of provenance and sedimentary processes. Mineralogical Society of America Reviews in Mineralogy 21, 169–200.
McLennan, S.M., Taylor, S.R., 1991. Sedimentary rocks and crustal evolution: tectonic setting and secular trends. Journal of Geology 99, 1–21.
Merino, E., Banerjee, A., 2008. Terra rossa genesis, implications for karst, and eolian dust: a geodynamic thread. Journal of Geology 116, 62–75.
Meshram, R.R., Randive, K.R., 2011. Geochemical study of laterites of the Jamnagar district, Gujarat, India: implications on parent rock, mineralogy and tectonics. Contents lists available at SciVerse Science Direct 42, 1271–1287.
Milnes, A.R., Fitzpatrick, R.W., 1989. Titanium and zirconium minerals. In: Dixon, J.B., Weed, S.W. (Eds.), Minerals in the Soil Environment. Soil Science Society of America, pp. 1131–1205.
Mongelli, G., 1993. REE and other trace elements in a granitic weathering profile from "Serre", southern Italy. Chemical Geology 103, 17–25.
Mordberg, L.E., 1993. Patterns of distribution and behaviour of trace elements in bauxites. Geochemical and Isotopic Record of Continental Weathering 107 (3–4), 241–244.
Mordberg, L.E., 1996. Geochemistry of trace elements in Paleozoic bauxite profiles in northern Russia. Geochemical Exploration 57, 187–199.
Morelli, F., Cullers, R., Laviano, R., Mongelli, G., 2000. Geochemistry and palaeoenvironmental significance of Upper Cretaceous clay-rich beds from the Peri-adriatic Apulia carbonate platform, southern Italy. Periodico di Mineralogia 69 (2), 165–183.
Moresi, M., Mongelli, G., 1988. The relation between the terra rossa and the carbonate-free residue of the underlying limestones and dolostones in Apulia, Italy. Clay Minerals 23, 439–446.
Muhs, D.R., Budahn, James R., 2006. Geochemical evidence for the origin of late Quaternary loess in central Alaska. Canadian Journal of Earth Sciences 43, 323–337.
Muhs, D.R., Budahn, James R., 2009. Geochemical evidence for African dust and volcanic ash inputs to terra rossa soils on carbonate reef terraces, northern Jamaica, west Indies. Quaternary International 196, 13–35.
Muhs, D.R., Budahn, J., Reheis, M., Beann, J., Skipp, G., Fisher, E., 2007. Airborne dust transport to the eastern Pacific Ocean off southern California: evidence from San Clemente island. Journal of Geophysical Research 112, D13203.1–D 13203.17.
Nakai, S., Halliday, A.N., Rea, D.K., 1993. Provenace of dust in the Pacific Ocean. Earth and Planetary Science Letters 119, 143–157.
Nesbitt, H.W., Markovics, G., 1997. Weathering of grandioritic crust, long-term storage of elements in weathering profiles, and petrogenesis of siliciclastic sediments. Geochimica et Cosmochimica Acta 61 (8), 1653–1670.
Nesbitt, H.W., Young, G.M., 1982. Early Proterozoic climates and plate motions inferred from major element chemistry of lutites. Nature 229, 715–717.
Olivarez, A.M., Owen, R.M., Rea, D.K., 1991. Geochemistry of eolian dust in Pacific pelagic sediments: Implications for paleoclimatic interpretations. Geochimica et Cosmochimica Acta 55 (8), 2147–2158.
Panahi, A., Young, G.M., Rainbird, R.H., 2000. Behavior of major and trace elements (including REE) during Paleoproterozoic pedogenesis and diagenetic alteration of Archean Granite near Ville Marie, Quebec, Canada. Geochimica et Cosmochimica Acta 64 (13), 2199–2220.
Parekh, P.P., Möller, P., Dulski, P., 1977. Distribution of trace elements between carbonate and noncarbonated phases of limestone. Earth and Planetary Science Letters 34 (1), 39–50.
Pearce, J.A., Cann, J.R., 1973. Tectonic setting of basic volcanic rocks determined using trace element analyses. Earth and Planetary Science Letters 19 (2), 290–300.
Peucker-Ehrenbrink, B., Jahn, B., 2001. Rhenium-osmium isotope systematics and platinum group element concentrations: loess and the upper continental crust. Geochemistry, Geo-699 physics, Geosystems 2 (10), 1061–1083.
Roaldset, E., 1973. Rare earth elements in Quaternary clays of the Numedal area, southern Norway. Lithos 6 (4), 349–372.
Roaldset, E., 1979. Rare earth elements in different size fractions of marine quick clay from Ullensaker, and a till from Upper Numedal, Norway. Clay Minerals 14, 229–240.
Savoy, L.E., Stevenson, R.K., Mountjoy, E.W., 2000. Provenance of upper Devonian–lower Carboniferous miogeoclinal strata, southeastern Canadian cordillera: link between tectonics and sedimentation. Journal of Sedimentary Research 70, 181–193.
Schellman, W., 1986. A new definition of laterite. In: Banerji, P.K. (Ed.), Lateritisation Processes. Geological Survey of India Memoir, 120, pp. 11–17.
Smedley, P.L., 1991. The geochemistry of rare earth elements in groundwater from the Carnmenellisarea, southwest England. Geochimica et Cosmochimica Acta 55 (10), 2767–2779.
Sun, J., 2002. Provenance of loess material and formation of loess deposits on Chinese Loess Plateau. Earth and Planetary Science Letters 203, 845–859.
Sušteršič, F., Rejšek, K., Mišič, M., Eichler, F., 2009. The role of loamy sediment (terra rossa) in the context of steady state karst surface lowering. Geomorphology 106, 35–45.
Taunton, A.E., Welch, S.A., Banfield, J.F., 2000. Geomicrobiological controls on light rare earth element, Y and Ba distributions during granite weathering and soil formation. Journal of Alloys and Compounds 303–304, 30–36.
Taylor, S.R., McLennan, S.M., 1985. The Continental Crust: Its Composition and Evolution. Blackwell Scientific Publications, Oxford (312 pp.).

Temur, S., Orhan, H., Deli, A., 2009. Geochemistry of the limestone of Mortas formation and related Terra Rossa, Seydisehir, Konya, Turkey. Geochemistry International 1, 72–97.
Turner, D.R., Whitfield, M., Dickson, A.G., 1981. The equilibrium speciation of dissolved components in freshwater and sea water at 25 °C and 1 atm pressure. Geochimica et Cosmochimica Acta 45 (6), 855–881.
Wang, L., Long, Y.Z., Peng, S.L., 2004. Geologic and geochemical study on material derivation of bauxite deposits in western Guangxi. Journal of Guilin University of Technology 24 (1), 1–6.
Watson, E.B., Green, T.H., 1981. Apatite/liquid partition coefficients for the rare earth elements and strontium. Earth and Planetary Science Letters 56, 405–421.
Wood, S.A., 1990. The aqueous geochemistry of the rare-earth elements and yttrium: 1. Review of available low-temperature data for inorganic complexes and the inorganic REE speciation of natural waters. Chemical Geology 82, 159–186.
Wu, G.Y., Yao, G.Y., 1997. A discussion on material source and metallogenic model of bauxite deposits in north china. Henan Geology 15 (3), 161–166 (in Chinese with English abstract).
Xu, L.Z., 2006. Geochemical characteristics of Emeishan basalt and mineralization of native copper deposit in junction area of Yunnan–Guizhou province, China. 16–24.
Young, G.M., Nesbitt, H.W., 1998. Processes controlling the distribution of Ti and Al in weathering profiles, siliciclastic sediments and sedimentary rocks. Journal of Sedimentary Research 68, 448–455.
Yu, L., Hou, E.G., Gao, Y.W., 2011. Progress of survey and research of Chinese bauxite deposit. Resources and Industries 13 (3), 27–33.
Zhong, H., Zhu, W.G., Qi, L., Zhou, M.F., Song, X.Y., Zhang, Y., 2006. Geochemical characteristics of platinum family element of Emeishan basalt in Panxi. Chinese Science Bulletin 15 (11), 1297–1304.